



4th International Workshop on Hydrogen and Fuel Cells

**within the 11th International Summer School on Advanced
Studies of Polymer Electrolyte Fuel Cells**

Graz University of Technology, August 23rd, 2018



4th International Workshop on Hydrogen and Fuel Cells

Thursday, 23rd August 2018

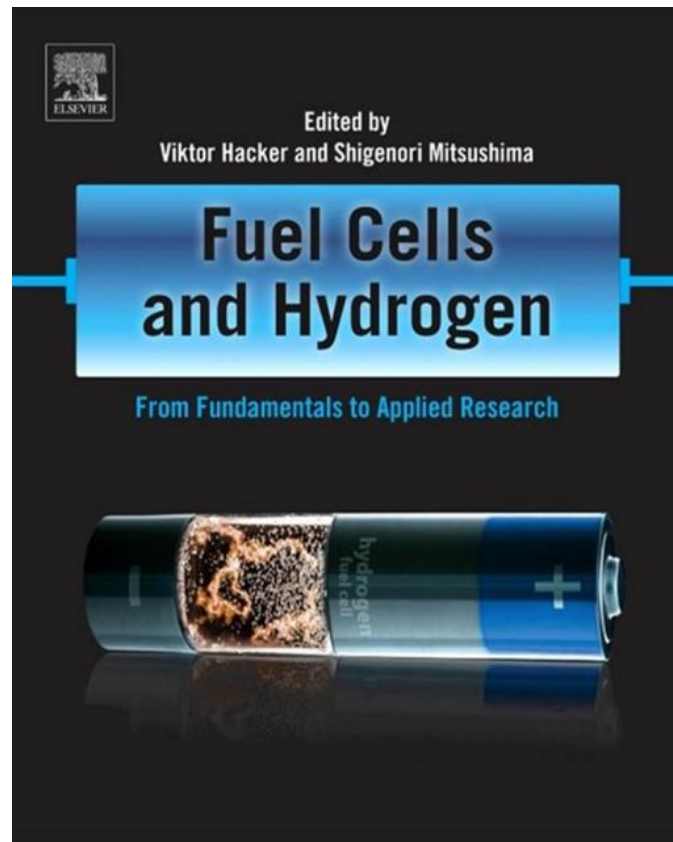
Graz University of Technology, Lecture Room i7

Inffeldgasse 25/D, 8010 Graz

Program

- 14:30 **Welcome**
Prof. Viktor HACKER, TU Graz
- Anion exchange membrane fuel cells**
Prof. Dario DEKEL, Technion,
Israel Institute of Technology, Haifa, Israel
- Industrialized production of PEM stacks and components**
Dr. Michael GÖTZ, ElringKlinger, Dettingen/Erms, Germany
- 3D Multiphysics Simulation of PEFCs – Modelling
Methodology and Selected Applications**
Dr. Reinhard TATSCHL, AVL List, Graz, Austria
- Fuel cells and hydrogen activities in Japan**
Prof. Ken-Ichiro OTA, Yokohama National University, Japan
- 16:15 **Student Poster Session**
- 17:15 **Get-together**
Catering sponsored by AVL List GmbH

Free admission when registered until 15.08.2018 at Brigitte.Hammer@TUGraz.at
Brigitte Hammer, Bakk.rer.soc.oec.
Institute of Chemical Engineering & Environmental Technology
Graz University of Technology



Fuel Cells and Hydrogen - From Fundamentals to Applied Research

Viktor HACKER, Shigenori MITSUSHIMA (eds.)

[ISBN: 9780128114599](https://doi.org/10.1016/C2018-0-00000-0), Elsevier 296 pages, 19th July 2018.

Fuel Cells and Hydrogen: From Fundamentals to Applied Research provides an overview of the basic principles of fuel cell and hydrogen technology, which subsequently allows the reader to delve more deeply into applied research. In addition to covering the **basic principles of fuel cells** and hydrogen technologies, the book examines the principles and methods to **develop and test fuel cells**, the evaluation of the **performance and lifetime** of fuel cells and the concepts of **hydrogen production**. *Fuel Cells and Hydrogen: From Fundamentals to Applied Research* acts as an invaluable reference book for **fuel cell developers** and **students**, researchers in **industry** entering the area of fuel cells and lecturers teaching fuel cells and hydrogen technology.

Contents

Poster Abstracts	3
<i>Prototype-scale hydrogen production from renewables via chemical-looping</i>	<i>4</i>
<i>Influence of biogas trace compounds on the purity of hydrogen production with the steam iron process</i>	<i>6</i>
<i>Characterisation of anode kinetics in alkaline fuel cells</i>	<i>9</i>
<i>Electrochemical analysis of reverse current in alkaline water electrolysis</i>	<i>11</i>
<i>New approach for enhancement of stability and oxygen reduction activity by ion implantation method.....</i>	<i>13</i>
<i>Numerical analysis of coagulation of water in PEFC cold start</i>	<i>15</i>
<i>Synthesis of nanostructured conductive titanium oxides by templating method.....</i>	<i>17</i>
<i>Influence of operating condition on current efficiency distribution in protonic ceramic fuel cell.....</i>	<i>19</i>
<i>Catalyst development to mitigate start-stop induced degradation in polymer electrolyte fuel cells.....</i>	<i>21</i>
<i>Electrochemical property of PtRu/C, Pt/C and IrRu/c cathode catalysts for toluene direct electro-hydrogenation.....</i>	<i>23</i>
<i>Predictive virtual methodology for performance and platinum degradation modelling of PEM fuel cells IN transient operating conditions.....</i>	<i>25</i>
<i>Steam reforming of bioethanol-gasoline mixtures.....</i>	<i>27</i>
<i>Titanium oxide nano-particles as supports of cathode catalysts for polymer electrolyte fuel cells.....</i>	<i>29</i>
<i>Experimental set-up for ethanol steam reforming</i>	<i>31</i>
<i>Structure dependence of OER activity in porous nickel electrode</i>	<i>33</i>
<i>Permeability of toluene and methylcyclohexane for proton exchange membrane.....</i>	<i>35</i>
<i>Total harmonic distortion analysis of flooding and dry out in simulations and experiments.....</i>	<i>37</i>
<i>FCEV system and driveline simulation analysis by using AVL Cruise M</i>	<i>39</i>
<i>Model electrode of oxygen reduction catalyst for PEFCs based on zirconium oxide by arc plasma deposition</i>	<i>41</i>

<i>Electrical efficiency and thermal autonomy of power generation system using protonic ceramic fuel cell.....</i>	<i>43</i>
<i>Activity of Pt-Pd catalysts supported on carbon black towards oxygen reduction reaction</i>	<i>45</i>
<i>Temperature measurement using thin film thermocouple during PEFC cold start</i>	<i>47</i>
<i>Manufacture and operation of 60 cm² zinc-air flow batteries with bifunctional air electrodes</i>	<i>49</i>
<i>Effects of the existence of MPL and GDL porosity to the local temperature and water distribution in PEFC</i>	<i>51</i>
<i>Effect of formation of electron conduction path on zirconia surface on oxygen reduction activity.....</i>	<i>54</i>
<i>Study of oxygen evolution reaction on zirconium oxide-based model electrode.....</i>	<i>56</i>
<i>Effect Of adding Nb to titanium oxides as non-platinum oxide-based cathodes for PEFC</i>	<i>58</i>
<i>New method for evaluation of powder OER catalysts for AWE.....</i>	<i>60</i>
<i>In situ electrochemical characterization of low-temperature PEM direct ethanol fuel cells using DC and AC methods.....</i>	<i>62</i>
<i>The effect of preparation conditions of Li_xNi_{2-x}O₂/Ni on electrochemical performance for alkaline water electrolysis</i>	<i>64</i>
<i>Development of iron based oxygen carriers for chemical looping hydrogen</i>	<i>66</i>
Keynote Speakers	68

Poster Abstracts

PROTOTYPE-SCALE HYDROGEN PRODUCTION FROM RENEWABLES VIA CHEMICAL-LOOPING

BOCK Sebastian¹, ZACHARIAS Robert¹, HACKER Viktor¹

¹ Institute of Chemical Engineering and Environmental Technology, Graz University of Technology, Austria, sebastian.bock@tugraz.at

Keywords: chemical looping, hydrogen production, biogas, steam iron process.

The reformer steam iron process (RESC) is a technology for decentralized on-site hydrogen production to upgrade biomass into a superior energy carrier for mobility applications [1]. At Graz University of Technology a unique integrated prototype reactor system was installed to demonstrate the applicability of the integral system for the conversion of different hydrocarbon feedstock [2].

INTRODUCTION

Current hydrogen production is predominantly performed by centralized large-scale steam reforming from fossil resources. Subsequently, the syngas is purified by pressure swing adsorption (PSA) and shipped or transported by truck in compressed or liquefied state over long distances. All these measures are cost- and energy intensive and linked with large emissions of CO₂ and other pollutants.

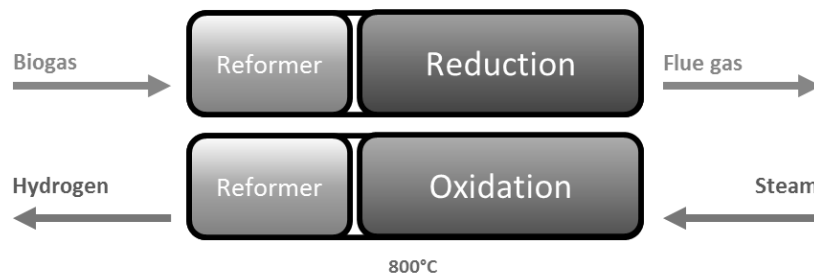
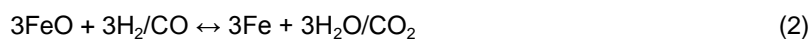
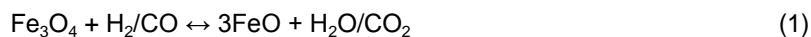


Figure 1: Simplified scheme of the RESC process for hydrogen production, adapted from [4].



Efficient hydrogen supply for mobility applications can be achieved by the decentralized and demand-oriented production in combination with an innovative purification process based on chemical looping hydrogen. Various hydrocarbon feedstock (e.g. biomass, biogas and others) can be converted to a high calorific syngas, reducing the iron-based oxygen carrier material in a reduction step [3]. Subsequently, steam oxidizes the iron-based material and a pure hydrogen stream is released (see Figure 1).

EXPERIMENTAL

A prototype reactor system with a steam reformer and fixed-bed chemical looping section was installed and heated with a gas burner to process temperatures of 800°C. The reactor is connected with a condenser and an Inficon MicroGC 3000 gas analyzer to determine the gas

impurities for the hydrogen product gas. The oxygen carrier used in this experiment is 300 g of dry mixed iron oxide with a 20% share of aluminum oxide as additive.

RESULTS

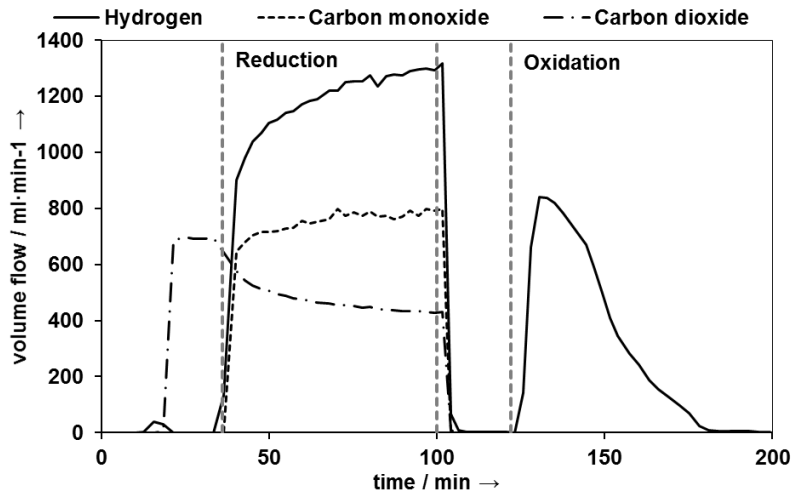


Figure 2: Dry gas composition during the reduction and oxidation phase in prototype lab-scale reactor system, adapted from [2].

A typical biogas composition (29.7% CH₄, 31.4% H₂O and 38.9% CO₂) was fed to the reactor system. In the reformer section, the gas is converted to a syngas mixture of hydrogen, carbon monoxide and carbon dioxide reducing the oxygen carrier material. During the reduction, the outgoing CO and H₂ concentration rises, since less oxygen carrier can be converted with longer reduction times. In the oxidation mode, pure hydrogen with a purity of 99.84% is released with an output power of 0.15kW based on hydrogen LHV.

Facing the high requirements for fuel cell electric vehicles (FCEV), requesting for a hydrogen purity exceeding 5.0 (99.999%), further experimental investigations and process improvements are projected. In addition to improve process applicability for renewables, advanced studies on typical contaminants occurring in biogas or gasified biomass are scheduled.

ACKNOWLEDGEMENTS

Financial support by the Klima- and Energiefonds through the Energy Research Program 2015 is gratefully acknowledged.

REFERENCES

- [1] V. Hacker, "A novel process for stationary hydrogen production: The reformer sponge iron cycle (RESC)", *J. Power Sources*, vol. 118 (2003), pp. 311–314.
- [2] S. Nestl, G. Voitic, R. Zacharias, S. Bock, and V. Hacker, "High-Purity Hydrogen Production with the Reformer Steam Iron Cycle," *Energy Technol.*, vol. 6 (2018), no. 3, pp. 563–569.
- [3] S. D. Fraser, M. Monsberger, and V. Hacker, "A thermodynamic analysis of the reformer sponge iron cycle", *J. Power Sources*, vol. 161 (2006), pp. 420–431.
- [4] S. Bock, R. Zacharias, V. Hacker, "Production of high purity hydrogen with a 10kWth RESC prototype system", in print (2018).

INFLUENCE OF BIOGAS TRACE COMPOUNDS ON THE PURITY OF HYDROGEN PRODUCTION WITH THE STEAM IRON PROCESS

DALVAI RAGNOLI Martin¹, BOCK Sebastian¹, ZACHARIAS Robert¹, HACKER Viktor¹

¹ Institute of Chemical Engineering and Environmental Technology, Graz University of Technology, Austria

Keywords: Hydrogen production, steam iron process, chemical looping, biogas, biomass

INTRODUCTION

Hydrogen is proposed as renewable secondary energy carrier to replace fossil hydrocarbons. The sustainability of hydrogen is determined by the production method. More than 90% of today's hydrogen is produced in centralised production plants and has to be transported over long distances. A process that comes along with considerable losses regarding the high volatility and the low volumetric energy density of hydrogen.

To avoid those drawbacks the reformer steam iron cycle (RESC) was proposed at Graz University of Technology. The process consists of a fixed bed chemical looping process to produce high-purity pressurized hydrogen from a broad range of renewable resources in decentralized applications. In a first step a metallic oxygen carrier is reduced with a reductive gas. Subsequently the metal is oxidised by steam. The latter process step produces fuel gas, a mixture of vapour and hydrogen [1],[2],[3].

EXPERIMENTAL

For decentralized on-demand hydrogen production the use of syngas from all different types of renewables (e.g. biogas, gasified biomass) as reductive gas is investigated. Since the composition of biogas or gasified biomass varies heavily based on the feedstock material, production method and season, a high flexibility of the process is needed. Besides the main components methane, carbon dioxide and nitrogen, biogas has a high amount of various trace compounds. Those include several volatile organic compounds as aromatic compounds (mostly benzene and toluene), sulphuric compounds (primarily hydrogen sulphide) and halogenated compounds as well as siloxanes. [4] [5]

Studying the influence of those trace compounds on the hydrogen purity when using biogas in the chemical loop hydrogen production is of crucial importance for the overall process feasibility. Hence model compounds are fed with the reductive gas in the reaction system during the reduction step. Methane and propane are selected as model compound for acyclic hydrocarbons, toluene to represent the cyclic hydrocarbons and hydrogen sulphide is to be substitutional for sulphuric components.

The carbon introduced in the reaction system during the reduction is expected to partly settle as elemental carbon. Carbon reacts subsequently to carbon monoxide or carbon dioxide with the oxygen provided by the steam during oxidation or accumulates and plugs the reactor. The sulphur could bond as metal sulphide in the oxygen carrier and hence deactivates it.

Table 1: Main and trace components of Biogas [5]

CH4	CO2	O2	N2	H2S	Halogenated compounds	Organic silicon compounds	Benzene	Toluene
[vol%]	[vol%]	[vol%]	[vol%]	[ppm]	[mg/m3]	[mg/m3]	[mg/m3]	[mg/m3]
40-70	30-40	<1	<1 - 20	1-1000	<0.1 - 1.3	<0.4 - 10	0.1 -2.3	0.2-11.8

The reactor consists of a stainless-steel tube with an inner diameter of 55 mm. The reactions take place at ambient pressure. Temperature is kept constant at 850 °C by an electrical furnace. The applied oxygen carrier contains 80% Fe₂O₃ and 20% Al₂O₃. The powders are dry mixed and pelletized and afterwards calcined in air at 900 °C for 6h. A layer of iron-based oxygen carrier material is embedded in the centre of the reactor to ensure a preheating zone for the inlet gases. The gaseous inlet fluids are regulated by mass flow controllers to guarantee exact feed composition. Water is supplied by a peristaltic pump and evaporated in a preheater. The weight difference between reduction and oxidation is constantly monitored and the dry flue gas is analysed with a MicroGC gas analytic system (Inficon Fusion).

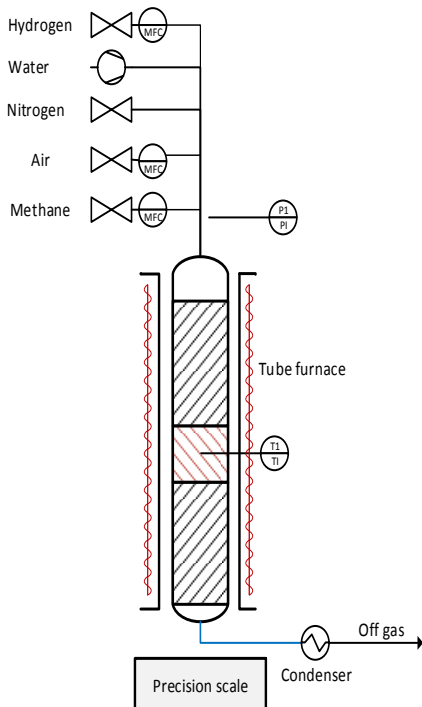


Figure 1: Flowsheet of experimental setup



Figure 2: picture of experimental setup

ACKNOWLEDGEMENTS

Financial support by the Klima- and Energiefonds through the Energy Research Program 2015 is gratefully acknowledged.

REFERENCES

- [1] S. Bock, R. Zacharias, and V. Hacker, "Production of high purity hydrogen with the fixed bed RESC process prototype."
- [2] S. Nestl, G. Voitic, R. Zacharias, S. Bock, and V. Hacker, "High-Purity Hydrogen Production with the Reformer Steam Iron Cycle," *Energy Technol.*, vol. 6, no. 3, pp. 563–569, 2018.
- [3] G. Voitic et al., "High purity pressurised hydrogen production from syngas by the steam-iron process," *RSC Adv.*, vol. 6, no. 58, pp. 53533–53541, 2016.
- [4] S. Rasi, A. Veijanen, and J. Rintala, "Trace compounds of biogas from different biogas production plants," *Energy*, vol. 32, no. 8, pp. 1375–1380, 2007.
- [5] S. Rasi, *Biogas Composition and Upgrading to Biomethane Saija Rasi Biogas Composition and Upgrading to Biomethane*. 2009.

CHARACTERISATION OF ANODE KINETICS IN ALKALINE FUEL CELLS

Maximilian Grandi¹, Anna Stark, Viktor Hacker

¹Institute for Chemical Engineering and Environmental Technology, Inffeldgasse 25C, 8010 Graz, Austria, maximilian.grandi@tugraz.at

Keywords: AFC, AEMFC, catalyst development, HOR kinetics

INTRODUCTION

The Alkaline fuel cell (AFC) was one of the first used for real applications. During the Apollo missions it provided power for the whole spacecraft. However, it used a liquid electrolyte and high Pt loadings. Since the development of new anion exchange membranes working in alkaline environments, there has been a revival of the (AFC) technology as Anion Exchange Membrane Fuel Cells (AEMFC) [1–3]. Due to the less corrosive environment and more favourable oxygen reduction kinetics, it is not necessary to use expensive platinum group metals (PGM) on the cathode [4,5].

However, the anode reaction kinetics prove to be more sluggish in alkaline environment, and in literature the catalysts mostly used is PtRu [3]. Another reason for this lack of catalysts, is the absence of an effective ex-situ characterisation method for the HOR needed for catalyst development. Because HOR kinetics are too fast, conventional Levich-analysis fails at the task [6]. Instead it is advisable to use the mass activity as exchange current density (i_0) per gram PGM used as comparison parameter. To obtain i_0 , the Koutecky-Levich Equation can be used to obtain the kinetic current i_k from rotating disk electrode (RDE) measurements and further perform Tafel-analysis on the data. To establish a method for effective comparison of different HOR catalysts PtRu/C was used as a benchmark catalyst, as it is the most found in literature.

EXPERIMENTAL

All measurements were performed in 0.1 M KOH as electrolyte and at 30°C. The benchmark PtRu/C catalyst was purchased from Alfa Aesar (40wt% Pt and 20wt% Ru) and suspended in a 7:3 water/1-propanol mixture. After adding 5wt% (of metal content) Nafion, the mixture was sonicated and drop coated onto the RDE to obtain a final loading of 28 $\mu\text{g}_{\text{PGM}} \text{cm}^{-2}$. Cyclic Voltammetry in nitrogen saturated electrolyte were performed, after which linear sweep voltammetry (LSV) was performed in hydrogen saturated electrolyte between 0 and 0.4 V vs RHE. Only data that showed linear Levich-plots was used for further analysis.

RDE-LSV currents obtained at 1600 rpm were corrected for iR -drop and then surface reactions with the CV in nitrogen saturated electrolyte. Using the Koutecky-Levich equation seen in equation the data was converted to the kinetic current density. A Tafel-plot was then created with the obtained values for J_k .

$$\frac{1}{J_m} = \frac{1}{J_D} + \frac{1}{J_K} = \frac{1}{0.62nFD^{2/3}\omega^{1/2}\nu^{-1/6}C} + \frac{1}{J_k} \quad (1)$$

RESULTS

The RDE-LSV curves corrected for iR drop and surface reactions and the Tafel-plot obtained which can be seen in

Figure 3. The fit to the linear region of the Tafel-plot was performed between 0.2 and 0.4 V vs RHE. It shows reasonably compatible with measurement data ($R^2=0.9927$).

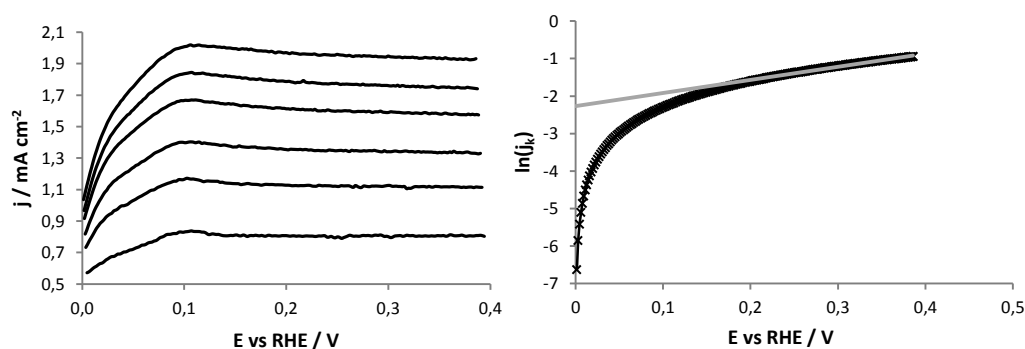


Figure 3: a) iR- and surface reaction corrected RDE-LSV diagram between 400 and 1600 rpm. b) Tafel-plot obtained from i_k at 1600 rpm.

The obtained mass activity using the exchange current density amounted to 13.4 A mg⁻¹PGM. Presented method has shown to be well suited for characterization of HOR kinetics in alkaline media.

REFERENCES

- [1] J.R. Varcoe, P. Atanassov, D.R. Dekel, A.M. Herring, M. a. Hickner, P. a. Kohl, A.R. Kucernak, W.E. Mustain, K. Nijmeijer, K. Scott, T. Xu, L. Zhuang, *Energy Environ. Sci.* 7 (2014) 3135–3191.
- [2] D.R. Dekel, 2016 Alkaline Membr. Fuel Cell Work., Phoenix, 2016.
- [3] S. Gottesfeld, D.R. Dekel, M. Page, C. Bae, Y. Yan, P. Zelenay, Y.S. Kim, *J. Power Sources.* (2017) 1–15.
- [4] I. Grimmer, P. Zorn, S. Weinberger, C. Grimmer, B. Pichler, B. Cermenek, F. Gebetsroither, A. Schenk, F.A. Mautner, B. Bitschnau, V. Hacker, *Electrochim. Acta.* 228 (2017) 325–331.
- [5] C. Grimmer, M. Grandi, R. Zacharias, S. Weinberger, A. Schenk, E. Aksamija, F. Mautner, B. Bitschnau, V. Hacker, *J. Electrochem. Soc.* 163 (2016).
- [6] W. Sheng, H.A. Gasteiger, Y. Shao-Horn, *J. Electrochem. Soc.* 157 (2010)

ELECTROCHEMICAL ANALYSIS OF REVERSE CURRENT IN ALKALINE WATER ELECTROLYSIS

Soki Hino¹, Kensaku Nagasawa², Yoshiyuki Kuroda¹ and Shigenori Mitsushima^{1,2}

¹Green Hydrogen Research Center, Yokohama National University, 79-5 Tokiwadai, Hodogaya-ku, Yokohama 240-8501, Japan, cel@ml.ynu.ac.jp

²Institute of Advanced Sciences, Yokohama National University, 79-5 Tokiwadai, Hodogaya-ku, Yokohama 240-8501, Japan, cel@ml.ynu.ac.jp

Keywords: Alkaline water electrolysis; Reverse current; Ni

INTRODUCTION

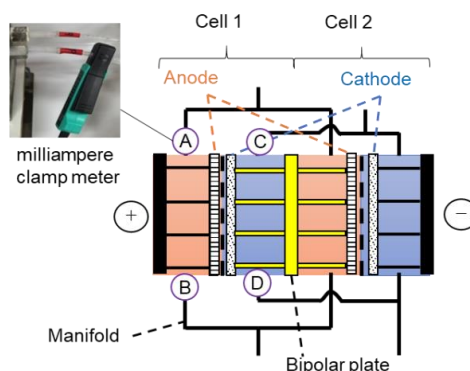
Water electrolysis has been paid attention to obtain hydrogen using the electricity generated from renewable energy. The electrode in electrolyzer needs the durability against the electric power fluctuation from renewable energy. In a bipolar type alkaline water electrolyzers, electrolyte solution is supplied from manifolds. Then, the leak current circuit by ionic conduction forms through the manifold. After electrolysis, the reverse current, which flows through the same manifold, causes the degradation of electrodes.¹⁾ When the nickel electrode is used in both anode and cathode, the reverse current originates from the reduction of NiOOH on anode and the oxidation of Ni, NiH, and H₂ on cathode.²⁾

In this study, we have investigated the relationship of the electrolysis time, the electrode potential, and the reverse current with a bipolar alkaline water electrolyzer. To evaluate the electrochemical behavior in the electrolyzer, the electrochemical measurement using three-electrode cell was also conducted.

EXPERIMENTAL

The bipolar electrolyzer consisted of two cells, which connected with the external manifold for electrolyte. Anode and cathode were Ni mesh, and Nafion membrane (NRE212CS) was used as the separator. The electrode area was 27.8 cm². A 7.0 M (=mol dm⁻³) NaOH solution was fed as the electrolyte to each electrode chamber at 25 ml min⁻¹. Electrochemical measurement in the bipolar electrolyzer was carried out as follows. External circuit opened after electrolysis for 10 s, 30, 60 or 120 min at 600 mA cm⁻². The reverse current in the manifold was measured with DC milliamper clamp meter. Reversible hydrogen electrodes (RHEs) were used as reference electrodes, and Luggin capillary was inserted near the cathode.

Three-electrode electrochemical cell measurement was conducted to analyze the reverse current. A working electrode was Ni mesh (geometric area: 1 cm²). A RHE and a coiled Ni were used as the reference and counter electrode, respectively. The electrolyte was 7.0 M NaOH. The anode and the cathode were scanned from the rest potential to 0.2 and 1.3 V after 600 or -600 mA cm⁻² electrolysis respectively. Electrolysis times were 10 s, 30, 60 and 120 min.



RESULTS AND DISCUSSION

Figure 1 shows the relationship between the electrode potentials and the charge of the reverse current on a bipolar plate of the electrolyzer. When electrolysis time was 30 min or longer, anode curves had the plateau at 1.3 V and dropped rapidly after that. When electrolysis time was 10 s, reverse current finished before the anode potential dropped, so the anode curve did not drop. However, it had the same plateau at 1.3 V as others.

Figure 2 shows the relationship between the electrode potentials and the charge after 600 and -600 mA cm⁻² electrolysis from 10 s to 120 min for the three-electrode cell using nickel mesh electrodes. The curves of the anode for the three-electrode cell had the same tendency for these of electrolyzer. The plateau at 1.3 V should correspond to the reaction from NiOOH to Ni(OH)₂; therefore, the amount of NiOOH was almost the same from 10 s to 120 min electrolysis.

The slopes of the cathodes in Figure 1 and 2 were the same tendency for the electrolyzer and the three-electrode electrochemical cell, which increased with decrease of the electrolysis time. The reduced species during electrolysis, such as Ni, NiH, and H₂ was oxidized by reverse current at the cathode,²⁾ so the cathode potential rises slowly, when there are a lot of reducing species. The amount of reducing species increases with the increase of electrolysis time.

The charge amounts of cathode and anode are the same during reverse current flows, because the redox reacts on the both sides of the bipolar plate. The anode and cathode potentials at some charge amount can be estimated. The anode and cathode potentials are important, because they are necessary for analyzing the reaction of degradation of electrodes by reverse current.

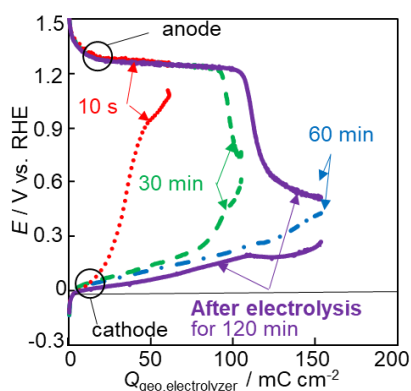


Fig. 1 The relationship between the electrode potentials and the charge of reverse current for the electrolyzer.

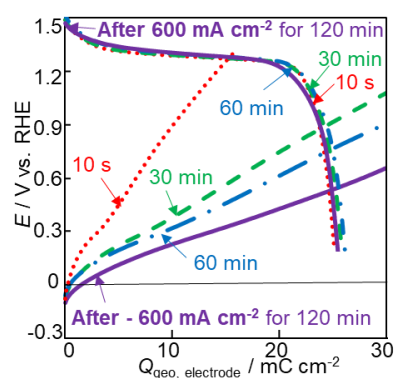


Fig. 2 The relationship between the electrode potentials and the charge after electrolysis for the three-electrode cell.

REFERENCES

- [1] V.D. Jovic, U. Lacnjevac, B.M. Jovic, N.V. Krstajic, *Electrochimica Acta*, 63, 124 (2012).
- [2] Y. Uchino, T. Kobayashi, S. Hasegawa, I. Nagashima, Y. Sunada, A. Manabe and S. Mitsushima, *Electrocatalysis*, 9, 67 (2018).

NEW APPROACH FOR ENHANCEMENT OF STABILITY AND OXYGEN REDUCTION ACTIVITY BY ION IMPLANTATION METHOD

J. Hirata¹, A. Ishihara², T. Nagai¹, Y. Kuroda¹, K. Matsuzawa¹, S. Mitsushima^{1,2}, and K. Ota¹

¹ Green Hydrogen Research Center, Yokohama National University (YNU), Hodogaya-ku, Yokohama, 240-8501 Japan, cel2@ml.ynu.ac.jp

² Institute of Advanced Sciences, YNU, Hodogaya-ku, Yokohama, 240-8501 Japan, cel2@ml.ynu.ac.jp

Keywords: oxygen reduction reaction, ion implantation, TiO₂ single crystal, polymer electrolyte fuel cell

INTRODUCTION

Although Polymer Electrolyte Fuel Cells (PEFCs) have high theoretical efficiency, the actual energy conversion efficiency to electricity is still low. In order to obtain more high efficiency and stability, the ORR activity and stability should be enhanced. We have focused on Group 4 and 5 metal oxide-based compounds, because their high stability in acidic electrolyte^[1]. However, the ORR activities of oxide-based cathodes are still much lower than that of platinum at present. We need to propose new strategy to enhance the ORR activities of oxide-based compounds.

On the other hand, it has been well known that the Fe-N bonding dispersed on the carbon support shows high ORR activity. However, the instability of Fe-N bonding was serious problem. Therefore, we think that Fe-N bonding would be stabilized by titanium oxide used as a stable matrix. We focused on ion implantation method to prepare the model electrode. Fe and N atoms were ion-implanted into the TiO₂ single crystal to evaluate the stability and the ORR activity.

EXPERIMENTAL

Nb (0.5 mol%) doped single-crystal rutile TiO₂ wafers (110) plane was used as a substrate of model electrode. The regulated flat surface was obtained by the following HF treatment^[2]. The surface of the (110) plane was washed with acetone and pure water, and immersed in 20 wt% HF for 10 min, and then rinsed with pure water and drying by nitrogen gas. The sample was annealed at 600 °C 150 min in air.

After HF treatment, the sample was ion-implanted at room temperature with 35 keV Fe ions and 10 keV N ions. After ion implantation, the samples were annealed in air or nitrogen for at 1300 °C 1 h to investigate the effect of heat-treatment.

In electrochemical measurement, in order to obtain conduction with single-crystal, Ga-In alloy was sandwiched between single-crystal and Au plate. Electrochemical measurements were performed in 0.1 mol dm⁻³ H₂SO₄ at room temperature. Cyclic voltammetry (CV) was carried out 300 cycles with a scan rate of 150 mV s⁻¹ from 0.05 to 1.2 V vs. RHE in N₂ atmosphere as pre-treatment. After CV, Slow Scan Voltammetry was carried out 8 cycles with a scan rate of 10 mV s⁻¹ from 0.2 to 1.2 V under N₂ and O₂ atmosphere. The ORR current density was calculated the difference current density between O₂ and N₂. In addition, the current divided by double layer capacity (C_{dl}) was defined $i_{\text{ORR}}/C_{\text{dl}}$. C_{dl} was calculated between 1.0 and 1.2 V in the cyclic voltammogram.

RESULTS AND DISCUSSION

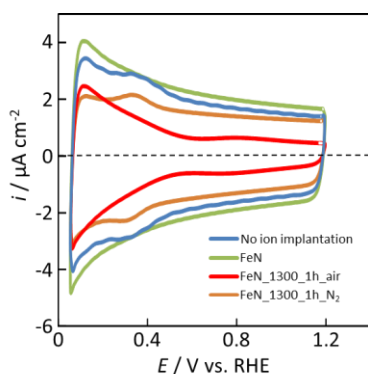


Fig.1 Steady-state CVs of no ion implantation and implantation samples

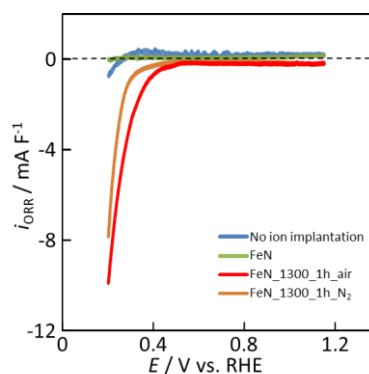


Fig.2 Potential-ORR current curve

Samples were made by ion implanting in the order of Fe and N. There is no large difference of the size of CV before and after ion implantation (Fig.1), suggesting that the surface of the substrate didn't get rough by ion implantation. In addition, although Fe was implanted, no anodic current was observed in the potential range from 0.05 to 1.2 V. This means the Fe ions might be stabilized into the TiO₂ matrix.

Fig.2 shows that the activity of the ion implanted sample (green line) without heat treatment was lower than that of the TiO₂ single-crystal (110) plane. Because the ions were driven into the substrate with high energy, the ions intruded not at the top surface but at a depth of approximately 8 nm from the surface. Needless to say, the catalytic reactions such as ORR occur at the top-surface of the catalysts. Therefore, the implanted ions intruded into the substrate did not increase the ORR activity. In addition, the implanted ions might exist interstitial sites instead of substitutional sites of Ti or O atoms.

Heat-treatment at high temperature such as 1300 °C was performed in order to diffuse the implanted ions from the inside of the substrate to the top-surface. As shown in Fig.2, the i_{ORR} increased approximately 8 times compared with the sample without ion implantation at 0.2 V. In particular, Heat-treatment under air enhanced the ORR activity. Furthermore, the onset potential increased by approximately 0.25 V by heat-treatment in air and N₂.

CONCLUSION

We proposed new approach for enhancement of stability and ORR activity by ion implantation method. We thought that Fe-N bonding would be stabilized by titanium oxide used as a stable matrix. Fe and N atoms were ion-implanted into the TiO₂ single crystal. We revealed that the heat-treatment at 1300 °C under air enhanced the ORR activity.

ACKNOWLEDGEMENT

The authors thank New Energy and Industrial Technology Organization (NEDO) for financial support. This work was supported by the Izumi Science and Technology Foundation, Tonen General Sekiyu Research / Development Encouragement & Scholarship Foundation, and JSPS KAKENHI Grant Number JP18K05291 and conducted under the auspices of the Ministry of Education, Culture, Sports, Science and Technology (MEXT) Program for Promoting the Reform of National Universities.

REFERENCES

- [1] J. H. Kim, A. Ishihara, S. Mitsushima, N. Kamiya, K. Ota, *Electrochim. Acta*, 52, 2492, (2007).
- [2] Y. Matsumoto, M. Katayama, *J. Surf. Sci. Japan*, 28, 10, 575, (2007).

NUMERICAL ANALYSIS OF COAGULATION OF WATER IN PEFC COLD START

Shoki INOUE¹, Yusuke TAMADA,² and Takuto ARAKI³

¹Graduate School of Eng., Yokohama National University, Japan, inoue-shoki-js@ynu.jp,

²Graduate School of Eng., Yokohama National University, Japan, tamada-yusuke-nt@ynu.jp,

³Faculty of Eng., Yokohama National University, Japan, taraki@ynu.ac.jp

Keywords: Numerical analysis, Coagulation, PEFC, below freezing temperature operation

INTRODUCTION

Polymer electrolyte fuel cell (PEFC) has attracted attention as a clean and highly efficient power generation system, and it is already in the stage of widespread use as a power source for automobiles and homes. One of the problems PEFC has is that PEFC can stop its operation at under-freezing temperature. It is thought that it is result of inhibiting supplying of reactive gas caused by product water coagulation at gas diffusion layer (GDL), catalyst layer (CL), and their interface [1]. And the formation of ice may damage the membrane, CL, and GDL [2]. However, it is not clearly understood how the subcooled product water moves and becomes ice in the cell. So, it is important to investigate a mechanism of ice formation and its effects in PEFC cold start. As an approach to that, there is a measuring a temperature change in the PEFC cold start focusing on heat of solidification [3]. This report aims to verify the temperature change by numerical analysis.

ANALYSIS MODEL

We used a simple one-dimensional heat conduction model. The governing equation is expressed by Eq.1,

$$\rho c \frac{\partial T}{\partial t} = k \frac{\partial^2 T}{\partial x^2} + s_r + s_c \quad (1)$$

where ρc is heat capacity of the materials, s_r is generation term by reaction, s_c is generation term by coagulation. s_r is the difference between the reaction enthalpy rate and the generated power. It is expressed as Eq.2,

$$s_r = \Delta_r H i / (2 F h_{CL}) - i V / h_{CL} \quad (2)$$

where $\Delta_r H$ is reaction enthalpy, i is generated current density, h_{CL} is thickness of catalyst layer (CL). The generation term by coagulation is uniform within a range where coagulation occurred, and it is given by the following Eq.3,

$$s_c = v \Delta_c H \quad (3)$$

where $\Delta_c H$ is latent heat, v is “coagulation rate”. For the coagulation time and the coagulation rate, the measurement result [3] was referred to. In addition, the heat capacity of the coagulation part is increased according to the amount of solidified water.

RESULT AND DISCUSSION

The analysis results are compared with the experimental measurements [3], which measured boundary temperature at both ends and two internal temperatures. Fig. 1 shows one of the results. ΔT is the temperature difference from the cathode separator which is the boundary condition. Because systematic errors may be included in the experimental measurements, the intercept of the experimental measurements is adapted to the temperature distribution obtained by analysis. The time at which coagulation, considered to be in measurement, started is set to 0. There are two ranges where coagulation occurs in MPL and CL to calculate, but there was no significant difference in the range.

There are some differences between analysis and measured results. One is the amount of change in ΔT between separator-GDL and MPL-CL. Another is temperature lowering rate after coagulation at MPL-CL. It seems that this is not the (at least, only) problem with the thermal diffusivity because the temperature rise at the two places is about the same in the measurement. Another possible cause is how to generate heat, that is, how to coagulate. Therefore, it is necessary to consider more about the coagulation mechanism.

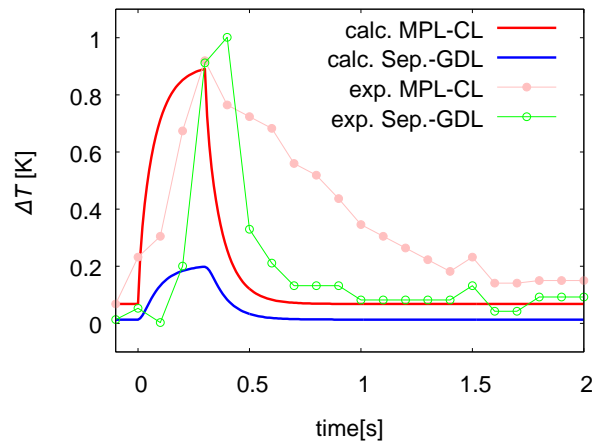


Fig. 1 Change of the temperature difference with cathode Sep.

REFERENCES

- [1] Y. Ishikawa et al. in: Journal of Power Sources, 179(2008), pp. 547-552
- [2] E.A. Cho et al. in: J. Electrochem. Soc., 150 (12) (2003), pp. A1667-A1670
- [3] Y. Tamada et al. in: The 55th National Heat Transfer Symposium, B132

SYNTHESIS OF NANOSTRUCTURED CONDUCTIVE TITANIUM OXIDES BY TEMPLATING METHOD

Hiroataka Kajima¹, Yoshiyuki Kuroda¹, Koichi Matsuzawa¹, Akimitsu Ishihara² and Shigenori Mitsushima^{1,2}

¹ Green Hydrogen Research Center, Yokohama National University, 79-5 Tokiwadai, Hodogaya-ku, Yokohama 240-8501, Japan

² Institute of Advanced Sciences, Yokohama National University, 79-5 Tokiwadai, Hodogaya-ku, Yokohama 240-8501, Japan
cel@ml.ynu.ac.jp

Keywords: conducting oxides, Nb-doped titanium oxides, porous materials, titanium suboxides

INTRODUCTION

The development of electrode materials with high durability is highly demanded because of increasing requirement of performances for commercial PEFC. In particular, the problem is the degradation of carbon materials in anode under high potential. Highly stable conductive metal oxides have attracted much attention as supports for substituting carbon materials in PEFC anodes. Conductive titanium oxides are useful materials because of their high stability and electroconductivity.^[1] Among them, the use of the Magnéli phase titanium suboxides, such as Ti_4O_7 , as catalyst supports on PEFC have frequently been reported. For example, Pt/ Ti_4O_7 showed high durability at 1.0 V-1.5 V vs. H_2 anode and specific activity for ORR. The stability was higher than those of carbon supports. However, the problem was low geometric current density due to low surface area.^[2] Although many efforts have been paid on the synthesis of mesoporous and macroporous titanium suboxides to increase surface area, those with both high surface area and high crystallinity have not been achieved, to the best of our knowledge. We have reported the synthesis of mesoporous titanium suboxides (Ti_4O_7 and Ti_6O_{11}) with high crystallinity, using mesoporous silica templates (SBA-15 and colloidal crystals),^[3] although the product contained some particles without porous structures probably because of the deposition of titanium oxides outside the templates. Here, we report the synthesis of highly ordered macroporous titanium suboxides without non-structured particles by seed-mediated hydrothermal templating method^[4] and subsequent hydrogen reduction of TiO_2 framework. We also found that the addition of niobium species is useful to synthesize highly ordered nanostructures, affecting hydrothermal crystal growth.

EXPERIMENTAL

A silica colloidal crystal, consisting of silica nanoparticles 70 nm in diameter, was synthesized according to the literature.^[6] Ti species, which acts as a seed of a TiO_2 framework, was formed in the colloidal crystal by heating the colloidal crystal in a 15 mM $TiCl_4$ solution 30mL, at 70°C for 1 h, followed by calcination at 550 °C for 30 min.^[4] The Ti-containing colloidal crystal was added in a solution, containing tetrabutoxytitanium (TBOT) 0.8 mL, $NbCl_5$ (0, 120, or 240 μ L for the Nb/Ti ratio of 0, 1, or 2 mol%), H_2O 28 mL and HCl 28 mL, and heated at 150 °C for 12 h.^[5] The sample with Nb/Ti ratio of 1 mol% was reduced by H_2 in a tube furnace with rotating sample room at 900°C for 5 h under H_2 flow at 230 mL/min. The template was removed in 2 M NaOH solution at 80°C for 2 h.

RESULT AND DISCUSSION

The SEM images of porous Nb- TiO_2 before reduction (Nb/Ti ratio = 0, 1, and 2 mol%) are shown in Fig.1. Morphologies of particles were different with the change in Nb/Ti ratio. The sample with Nb/Ti = 0 mol% has highly anisotropic shape (rod-like shape), though those with Nb/Ti = 1 and 2 mol% have relatively isotropic shapes. The particle size of the sample with Nb/Ti = 2 mol% was

smaller than other samples. The XRD patterns of the samples with Nb/Ti ratio = 0 and 1 mol% exhibited the peaks attributed to rutile, brookite and anatase, whereas that with Nb/Ti = 2 mol% exhibited only anatase. It is known that increase in the Nb/Ti ratio suppresses the transformation from anatase to rutile at high temperature.^[7] The formation of anatase phase in this study at Nb/Ti = 2 mol% is possibly due to the similar effect of the stabilization of anatase phase.

The lattice constants (*a* and *c*) and cell volume increased along with the Nb/Ti ratio, which suggests successful incorporation of Nb in the TiO₂ framework.^[7] Highly ordered porous Ti₄O₇ was synthesized by H₂ reduction after the hydrothermal deposition of Nb-doped TiO₂ in the template. The Nb/Ti ratio was chosen to be 1 mol% because highly ordered nanostructure was formed in this condition without the H₂ reduction. The XRD pattern exhibited many peaks attributed to Ti₄O₇ and some weak peaks attributed to anatase (Fig. 2), showing successful transformation of TiO₂ framework to the titanium suboxide. The presence of a small amount of anatase is probably due to difficulty of reduction of confined TiO₂ in the template. The SEM image of the reduced sample showed highly ordered porous structure (Fig.3). The N₂ adsorption-desorption isotherm was type IV with a hysteresis, corresponding to a sort of a mesoporous material with large pore (ca. 68 nm). The BET specific surface area was 46 m²g⁻¹ that is almost the same as that of the porous TiO₂ without H₂ reduction, suggesting that the H₂ reduction was less influential to the deformation of nanostructures in a template.

In conclusion, nanostructured conductive titanium suboxide with highly ordered macroporous structure was successfully synthesized by the seed-mediated hydrothermal templating method.

REFERENCES

- [1] B. Xu, et al., RSC Adv, 6, 79706 (2016).
- [2] T. Ioroi, et al., J. Electrochem. Soc., 155, B321 (2008).
- [3] Igarashi et al., The 58th Battery Symposium in Japan, 2F03, (2017)
- [4] E. J. W. Crossland et al., Nature. 495, 215 (2013).
- [5] M. Kitahara et al., Chem. Eur. J. 21, 13073 (2015).
- [6] K. M. Choi and K. Kuroda, Chem Commun., 47, 10933, 2011.
- [7] V. Guidi et al., J. Phys. Chem. B, 107, 120 (2003).

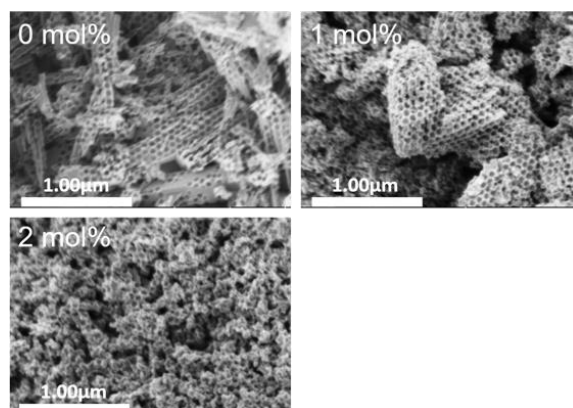


Fig.1. SEM images of nanostructured titanium oxide with different Nb/Ti ratio (0 mol%, 1 mol% and 2 mol%).

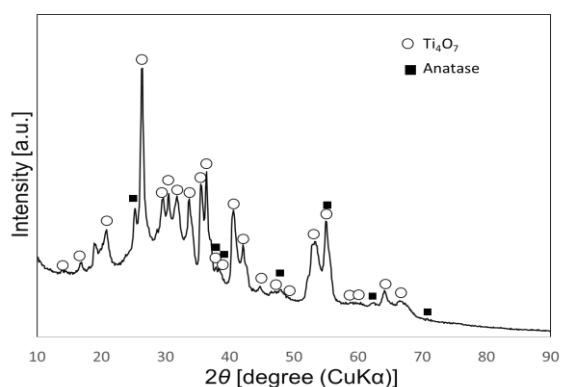


Fig.2. X-ray diffraction pattern of nanostructured Ti₄O₇ (Nb/Ti = 1 mol% reduced by H₂).

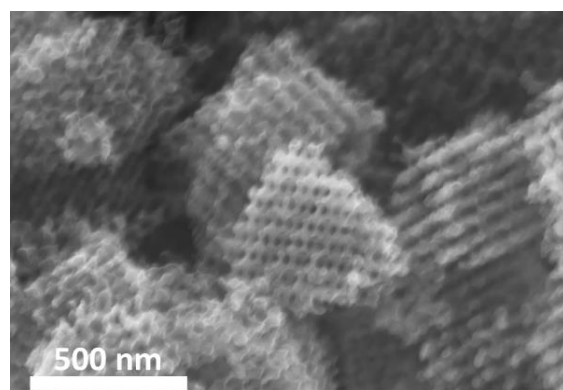


Fig.3. SEM image of nanostructured Ti₄O₇ (Nb/Ti = 1 mol% reduced by H₂).

INFLUENCE OF OPERATING CONDITION ON CURRENT EFFICIENCY DISTRIBUTION IN PROTONIC CERAMIC FUEL CELL

Toshiki Kawamura¹, Kunpeng Li², Takuto Araki³, Yuzi Okuyama⁴

¹ Graduate School of Engineering, Yokohama National University, Japan, kawamura-toshiki-dh@ynu.jp

² Graduate School of Engineering, Yokohama National University, Japan, li-kunpeng-pt@ynu.jp

³ Faculty of Engineering, Yokohama National Engineering, Japan, taraki@ynu.jp

⁴ Department of Environmental Robotics, Faculty of Engineering, Miyazaki University, Japan, okuyama@cc.miyazaki-u.ac.jp

Keywords: Protonic ceramic fuel cell (PCFC), Hole, Current efficiency, Numerical analysis

INTRODUCTION

Solid oxide fuel cells (SOFCs) are electrochemical devices that can achieve the high electrical efficiency under high operating temperatures compared to other types of fuel cells. Currently, oxide ion-conductive type SOFCs is widely used. In order to improve the electrical efficiency using SOFCs, it is conceivable to operate under high fuel utilization ratio. However, in the case of using oxide-ion conducting SOFCs, fuel is diluted by produced water vapor when operating under high fuel utilization ratio. On the other hand, in the case of using protonic ceramic fuel cells (PCFCs), fuel dilution does not occur since the generation of water vapor by the electrochemical reaction takes place on the air electrode side. Furthermore, PCFCs have a high ion conductivity in the middle temperature range (773.15~973.15K). So, it is possible to reduce the cost of balance of plant (BoP). According to Matsuzaki et al. [1], it is shown that high fuel utilization ratio is maintained and high electrical efficiency exceeding 80% (LHV) is theoretically possible. Proton conductive electrolyte is a mixed conducting material that conducts not only proton but also oxide ion, hole, and electron [2]. Especially, hole conduction reduces local faradaic efficiency in the middle temperature range. Current proportion of proton and hole is influenced by gas flow direction, gas utilization rate and electrolyte thickness. In this study, we investigated the effect of temperature distribution, gas concentration distribution and the geometry on the currents of proton and hole.

NUMERICAL ANALYSIS MODEL AND CONDITION

Several different proton conductive materials showed the ability to absorb water vapor and oxygen and generate electron holes. In the present study, we suppose $\text{BaZr}_{0.2}\text{Yb}_{0.8}\text{O}_{3-\delta}$ (BZYb) as the electrolyte material of our PCFC model. In addition to the two traditional half-reactions at electrodes, the hole generating reactions, proton generating reactions, and the reactions between electron and electron holes take place simultaneously between materials and atmospheres under wet condition. These reactions induce current leakage, and we use $\phi_{\text{current}} = I_{\text{external}}/I_{\text{H}}$ to express the local current efficiency. I_{external} and I_{H} are the current density through external circuit and proton current density, respectively. The control equation of current efficiency was derived and shown as follows.

$$\phi_{\text{current}} = 1 + \frac{\sigma_{\text{h}}^0}{\sigma_{\text{H}}^0} \left(\frac{(P_{\text{O}_2(\text{anode})})^{1/4} \exp\left(\frac{I_{\text{H}} L F}{RT \sigma_{\text{H}}^0}\right) - (P_{\text{O}_2(\text{cathode})})^{1/4}}{\exp\left(\frac{I_{\text{H}} L F}{RT \sigma_{\text{H}}^0}\right) - 1} \right) \quad (1)$$

where, ϕ_{current} is current efficiency. σ_{h}^0 and σ_{H}^0 are conductivities of hole and proton in electrolyte, respectively. $P_{\text{O}_2(\text{anode})}$ and $P_{\text{O}_2(\text{cathode})}$ are partial pressures of oxygen at anode and cathode side, respectively. I_{H} is the proton current density. L is the thickness of electrolyte. T is the operating absolute temperature of fuel cell. F is Faraday's constant, and R is ideal gas constant. Numerical conditions are shown in Table 1.

Table 1. Calculation conditions of base case

Parameters	Values	Units
Operating temperature	873.15	K
H ₂ / Air flow rate (3%H ₂ O)	10, 32	mL/min
Operating pressure	1.0	atm
Utilization of H ₂ and O ₂	60, 30	%
Operating voltage	0.78	V
I_{H}	0.3	A/cm ²
L	20	μm

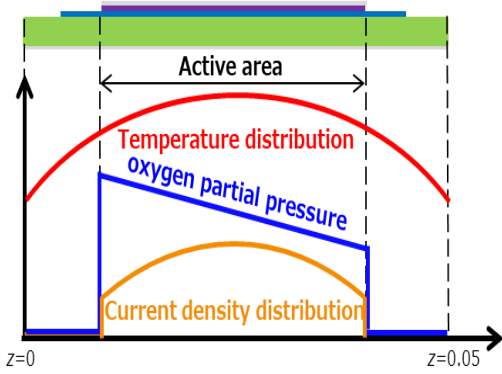


Figure 1. Relationship of each distribution

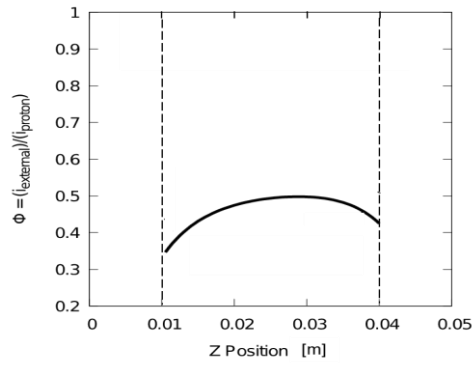


Figure 2. Current efficiency distribution

RESULT AND DISCUSSIONS

In consideration of the effect of Oxygen partial pressure, temperature, and current density distribution, the current efficiency distribution in cell axis direction was calculated. Each distribution in cell axis direction is shown in Fig. 1, and current efficiency distribution in the same direction is shown in Fig. 2. Since oxygen is consumed by the electrochemical reaction, the oxygen partial pressure distribution decreases toward the downstream. So, current efficiency distribution tends to rise to the right as a whole because hole conductivity is proportional to the 1/4 power of the oxygen partial pressure as seen in equation (1). Since both ends of the cell are in isothermal state, the temperature distribution tends to rise in the center part and the current density distribution also becomes the same. Due to these influences, the current efficiency increased in the central part of the cell. In addition, current efficiency should change depending on the electrolyte thickness etc.

Suppressing hole current becomes important to improve electrical efficiency. Therefore, various parameters are effective for current efficiency (ultimately, electrical efficiency), so setting appropriate parameters and operating conditions is necessary in PCFC.

REFERENCES

- [1] Y. Matsuzaki, Y. Tachikawa, et al., Scientific Reports, 5(1), 12640(2015).
- [2] E. Fabbri, D. Pergolesi, et al., Chemical Society Reviews, 39(11), 4355-4369(2010).

CATALYST DEVELOPMENT TO MITIGATE START-STOP INDUCED DEGRADATION IN POLYMER ELECTROLYTE FUEL CELLS

Katharina KOCHER¹, Viktor HACKER¹

¹ Graz University of Technology, Institute of Chemical Engineering and Environmental Technology, Inffeldgasse 25/C, 8010 Graz, Austria
katharina.kocher@tugraz.at

Keywords: PEFC, catalyst degradation, Polyaniline, durable ORR catalyst, rotating disk electrode analysis

INTRODUCTION

Lifetime of polymer electrolyte fuel cells (PEFCs) for automotive applications is one of the major issues restricting its successful commercialization. Under real driving cycles four main operations conditions cause FC degradation: load change, high power, idling and start-stop (Fig. 1).

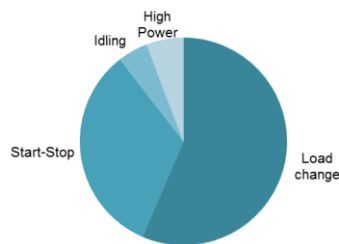


Fig. 1: PEM FC degradation caused by automotive operation conditions

The main reason for performance degradation during start-stop process is the formation of a hydrogen/air interface. Its presence leads to oxidation reaction in the anode, further causing high potentials of up to 1.44 V at the cathode [1]. This phenomenon leads to severe cathode catalyst failure, as it accelerates carbon support corrosion, platinum agglomeration as well as platinum dissolution. As a result the catalyst's electrochemical active surface area (ECSA) and oxygen reduction reaction (ORR) activity decrease.

Considering the whole FC system, alternative control and operation strategies can approach an improvement in robustness. However, in the long term and in order to mitigate start-stop induced material degradation, it is desirable to develop and implement new catalyst materials toward durable PEFCs.

For this purpose, functionalized catalysts based on platinum (Pt), carbon (C), and a conducting polymer, i.e. polyaniline (PANI), were developed (Fig.2). Thereby the PANI forms a protective thin film around the catalyst particles (Pt/C@PANI). Through an electron transfer between the Pt

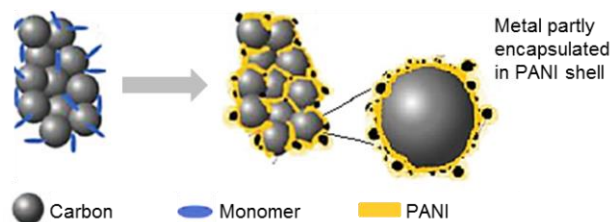


Fig. 2: Schematic synthesis of Pt/C@PANI

d-orbitals and the π -conjugated electron system of the polymer surrounding the carbon, the interaction between the support and metal as well as the carbon corrosion resistance is increased, subsequent enhancing the catalyst's activity and stability.

EXPERIMENTAL

A Pt/C@PANI catalyst was synthesized through oxidative polymerization of aniline monomers [2]. The prepared catalyst was ex-situ characterized by means of thin film rotating disk electrode technique using a standard three electrode set-up. In order to determine the ECSA and the ORR activity (mass activity, MA), cyclic voltammetry (CV) and ORR measurements were recorded in N_2 and O_2 purged electrolyte, respectively.

RESULTS AND OUTLOOK

Compared to a commercial Pt/C catalyst, Pt/C@PANI shows a slightly increased ECSA of $1.3 \pm 0.1\%$ and a significant improvement in MA of about $57 \pm 0.1\%$ (Fig.3).

In order to investigate the protective effect of the PANI film against start-stop cycling, the next focus will be on specific RDE experiments, which simulate these start-stop conditions, to evaluate the stability, i.e. the robustness, of the new functionalized catalyst.

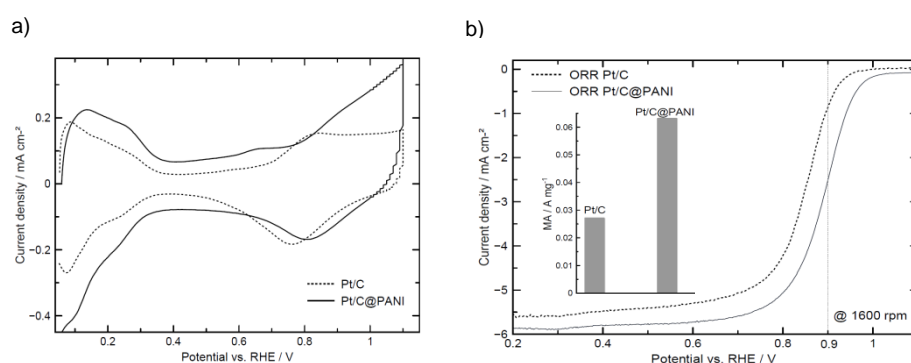


Fig. 3: a) CV curves and b) ORR activity measurement of Pt/C and Pt/C@PANI catalyst

ACKNOWLEDGMENTS

Financial support was provided by The Climate and Energy Fund of the Austrian Federal Government and The Austrian Research Promotion Agency (FFG) through the program Energieforschung (e!Mission) and the IEA research cooperation.

REFERENCES

- [1] T. Zhang et al., "A review of automotive proton exchange membrane fuel cell degradation under start-stop operation conditions", *Applied Energy*, 223 pp. 249-262, 2018
- [2] S. Chen et al., "Nanostructured polyaniline-decorated Pt/C@PANI core-shell catalyst with enhanced durability and activity," *J. Am. Chem. Soc.*, vol. 134, pp. 13252–13255, 2012

ELECTROCHEMICAL PROPERTY OF PtRu/C, Pt/C AND IrRu/C CATHODE CATALYSTS FOR TOLUENE DIRECT ELECTRO-HYDROGENATION

Junpei Koike,¹ Kensaku Nagasawa,² Yuta Inami,³ Ichiro Yamanaka,³ Yoshiyuki Kuroda,¹ Koichi Matsuzawa,¹ and Shigenori Mitsushima^{1,2}

¹ Green Hydrogen Research Center, Yokohama National University, 79-5 Tokiwadai, Hodogaya-ku, Yokohama 240-8501, Japan

² Institute of Advanced Sciences, Yokohama National University, 79-5 Tokiwadai, Hodogaya-ku, Yokohama 240-8501, Japan

³ School of Materials and Chemical Technology, Tokyo institute of technology, 2-12-1 Ookayama, Meguro-ku, Tokyo, Japan
E-mail: cel@ml.ynu.ac.jp

Keywords: Pt/C, PtRu/C, IrRu/C, toluene direct electro-hydrogenation

INTRODUCTION

Recently, utilization of renewable energy has been expected to decrease the carbon dioxide emission. For effective utilization of the fluctuated and uneven distributed renewable energy, the large-scale storage and transportation of hydrogen as secondary energy is needed. In the candidates of energy carrier, toluene(TL)/ methylcyclohexane(MCH) organic chemical hydride system has the advantages of efficiency, safety and handling, because TL and MCH are a liquid at ambient temperature and pressure, and will be able to use oil infrastructure. We have studied the high-efficient electrolytic direct-hydrogenation of toluene with water decomposition for the organic hydride system as an efficient energy carrier process.^{1,2} This method has the advantages of lower theoretical decomposition voltage and no exothermic heat loss compare with the conventional 2-step TL hydrogenation after the water electrolysis. In this study, to improve electrochemical properties for cathode catalysts, PtRu/C, Pt/C and IrRu/C has been compared.

EXPERIMENTAL

A DSE[®] electrode for the oxygen evolution (De Nora Permelec Ltd), 0.5 mg_{-metal} cm⁻² of PtRu/C (Pt : 30.2 wt%, Ru : 23.4 wt%, TEC61E54, Tanaka Kikinzoku Kogyo (TKK)), Pt/C (Pt : 47.2 wt%, TEC10E50E, TKK) or in-house IrRu/C (Ir : 5.0 wt%, Ru : 5.0 wt%, Ketjenblack, KB) catalyst with ionomer applied a carbon paper (10BC, SGL group -The Carbon Co.) and Nafion 117[®] (Du Pont) were used for the anode, the cathode, and the proton exchange membrane (PEM), respectively. The IrRu/C catalyst was prepared by impregnation method, which KB mixed IrCl₃ · 3H₂O and RuCl₃ · 3H₂O aqueous solution was reduced by NaBH₄.² The carbon paper as the diffusion layer was loaded 0.02 mg_{-Pt} cm⁻² of Pt particles by the impregnation method. The cathode was hot-pressed on the PEM at 120 °C and 4 MPa for 3 min to fabricate a membrane cathode assembly. The cathode flow fields were porous-carbon flow path of the 10BC. Operation temperature of the electrolyzer conducted at 60 or 80°C. The anode and cathode compartments were circulated 1 mol dm⁻³ H₂SO₄ and 10 or 100% TL/MCH, respectively. The electrochemical measurements were conducted for the linear sweep voltammetry (LSV), the electrochemical impedance spectroscopy (EIS), the chronoamperometry (CA) and the Faraday efficiency measurement.

RESULTS AND DISCUSSION

Figure 1 shows the results of LSV measurements at 60°C and 80°C with 10% TL feed. At 400 mA cm⁻², the PtRu/C at 60°C and Pt/C at 80°C were the lowest cell voltage at each temperature. The IrRu/C exhibited the highest cell voltage at both temperature. However, the low performance of the IrRu/C would be for the influence of internal resistance. Compared to the PtRu/C and the Pt/C, the IrRu/C had a high ratio of carbon support. Therefore, the catalyst layer became thicker to get same precious metal loading. For this reason, undulation occurred on the surface of the catalyst layer, and the internal resistance of the IrRu/C would be higher than others.

Figure 2 shows the cathode polarization curves with 10 %TL at 60 and 80°C. Obvious differences for cathode potentials of each catalyst were not observed at 60°C. On the other hand, the IrRu/C and Pt/C at 80°C were lower overpotential than the PtRu/C. Especially, more than 250 mA cm⁻², the IrRu/C was the lowest overpotential. The difference in overpotential at each temperature would be caused by the changes in the balance of hydrogen and toluene adsorption ability on each atomic metal surface of catalyst with temperature. In high current density region over 500-600 mA cm⁻², the overpotential was affected by mass transfer, so the IrRu/C catalyst layer seems to be effective for TL transfer. Open circuit potentials, which reflect the intrinsic activity of catalyst, were IrRu/C > PtRu/C ≥ Pt/C at 80°C and IrRu/C > Pt/C ≥ PtRu/C at 60°C. IrRu/C would show the high potential for toluene hydrogenation catalyst due to the high hydrogen adsorption ability on Ir atomic surface³. From the above, the IrRu/C showed high performance due to adsorption balance of TL and H₂ of precious metal in TL direct electrohydrogenation, while mass transfer by precious metal and carbon support composition would be considered.

ACKNOWLEDGEMENTS

This work was supported by New Energy and Industrial Technology Development Organization (NEDO) and Toyota Mobility Foundation. The Institute of Advanced Sciences (IAS) in YNU is supported by the MEXT Program for Promoting Reform of National Universities.

REFERENCES

- [1] S. Mitsushima, Y. Takakuwa, K. Nagasawa, Y. Sawaguchi, Y. Kohno, K. Matsuzawa, Z. Awaludin, A. Kato, and Y. Nishiki, *Electrocatalysis*, 7, 127 (2016).
- [2] K. Nagasawa, Y. Sawaguchi, A. Kato, Y. Nishiki, S. Mitsushima, *Electrocatalysis* 8, 164 (2017).
- [3] Y. Inami, H. Ogihara, I. Yamanaka, *ChemistrySelect*, 2, 1939 (2017).

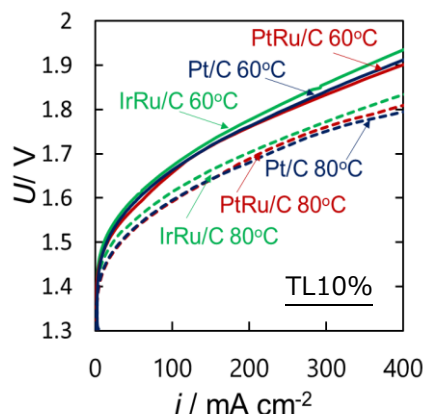


Figure.1 LSV curves with 10% toluene at 60°C and 80°C.

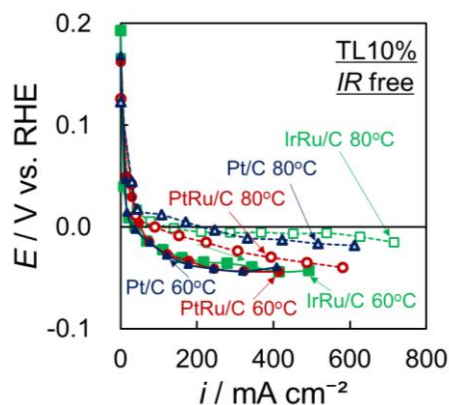


Figure.2 Cathode polarization curves with 10 % toluene at 60 and 80°C.

PREDICTIVE VIRTUAL METHODOLOGY FOR PERFORMANCE AND PLATINUM DEGRADATION MODELLING OF PEM FUEL CELLS IN TRANSIENT OPERATING CONDITIONS

Andraž Kravos^{1,2}, Ambrož Kregar^{1,3}, Gregor Tavčar^{1,4} and Tomaž Katrašnik^{1,5}

¹ University of Ljubljana, Faculty of Mechanical Engineering, Aškerčeva 6, SI-1000 Ljubljana, Slovenia, ² andraz.kravos@fs.uni-lj.si, ³ ambroz.kregar@fs.uni-lj.si, ⁴ gregor.tavcar@fs.uni-lj.si and ⁵ tomaz.katrasnik@fs.uni-lj.si.

Keywords: Fuel cell; Proton exchange membrane; Modelling; Predictive; Platinum degradation

ABSTRACT

Polymer electrolyte membrane fuel cells (PEMFCs) are a promising and emerging clean energy conversion technology for mobile and stationary applications. Simultaneous reduction of production costs and prolongation of the service life are considered to be significant challenges towards their wider market adoptions. These challenges call for application of predictive virtual tools during the development process of PEMFC systems.

In order to achieve significant progress in the addressed area, this contribution presents an innovative modelling framework based on: a) a mechanistically based spatially and temporally resolved PEMFC performance model and b) a modular degradation modelling framework based on interacting partial degradation mechanisms.

The core principle of the physically based spatially and temporally resolved PEMFC performance model is a novel computationally efficient approach combining a 1D numerical and a 2D analytic solution, denoted Hybrid 3D Analytic-Numerical (HAN) which is fully presented in [1,2]. Further on, a computationally optimized version of HAN was developed and presented in [3] that complies with real-time constraints denoted HAN-RT. HAN modelling approach thus on one hand allows for achieving high level of predictiveness in FC performance modelling, which is crucial for an adequate virtual integration of FC in the plant model, and on the other hand provides spatially and temporally resolved data of degradation stimuli, which are the required input parameters for the degradation modelling framework.

The modular degradation modelling framework considers in an interacting manner partial degradation mechanisms such as: carbon and Pt oxidation phenomena and Pt dissolution, redeposition, detachment and agglomeration phenomena (Fig.1(left)), which are further on integrated into adequate causal chains for simulating degradation of electrochemical devices.

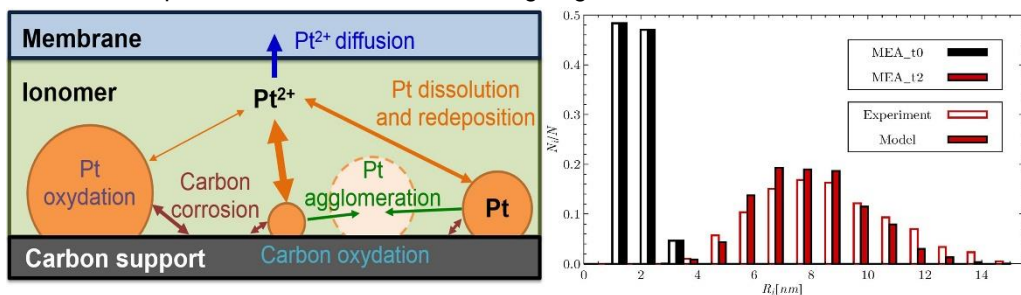


Fig. 1: A schematic diagram of the intertwined degradation mechanisms. (left) The comparison between experimentally measured particle size distribution (white-filled histogram) and the one produced by degradation model (coloured histogram) for fresh and aged MEA. (right)

The degradation model was validated against the experimental data from [4], where a HT-PEM fuel cell was operated at steady state conditions for 4800 hours (MEA_t2), with the focus on the changes in particle size distribution. The input variables of the degradation model were: a) experimentally measured particle size distribution of a fresh sample (MEA_t0) and b) data on local conditions on catalyst surface using the FC performance model simulation replicating the same operating conditions as used in the experimental setup of [4]. In Fig. 1 (right), results of the particle size distribution simulated by the proposed degradation model are compared to the experimentally measured particle size distribution of the degraded cells, exhibiting remarkable agreement, thereby confirming credibility of the model. The validated modelling framework was then used in a transient degradation analysis following the protocol given in [5]. The fuel cell voltage was cycled between 0.6 and 0.96 V every 30 seconds and the results were compared to a constant high voltage operation at 0.96 V. The resulting relative rise in mean Pt particle size is shown in black in Fig.2 (right) and indicates faster particle growth in voltage cycling regime. As seen by comparing the two contributions to the particle redistribution, i.e.: due to particle detachment (green line) and dissolution (blue line), faster growth rate can be attributed to the detachment due to carbon corrosion, which is much more pronounced in the voltage cycling regime. This can be further explained by the accumulation of C-OH groups (red line - Fig.2 (left)) during the periods of low voltage and their interaction with Pt-OH groups during the periods of high voltage.

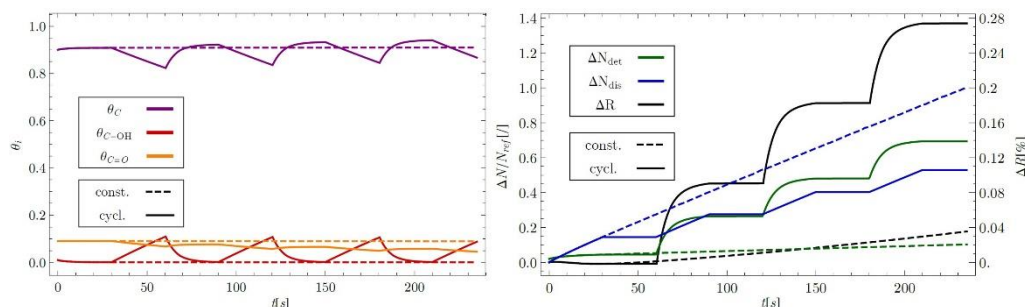


Fig. 2: Dynamics of surface oxides and hydroxides on carbon support. (left) Relative change in mean particle size (black) due to detachment (green) and dissolution (blue) with time for voltage cycling and constant high voltage operation. (right)

Compared to the current state of the art and owing to its structured basis that covers the entire causal chain from FC operation and control over prediction of FC performance and degradation stimuli to prediction of degradation rates over longer time scales, the proposed innovative modelling framework enables more efficient exploration of the design space and offers a higher fidelity model to support the design of FC systems including their control functionalities.

REFERENCES

- [1] G. Tavčar and T. Katrašnik: *Energies* Vol. 6 (10), (2013), p. 5426-548
- [2] G. Tavčar and T. Katrašnik: *Acta chimica slovenica* Vol. 61 (2), (2014), p. 284-301
- [3] G. Tavčar and T. Katrašnik: 5th EUROPEAN PEFC&H2 FORUM, 30.6.– 3.7. 2015
- [4] K. Hengge, C. Heinzl, M. Perchthaler, D. Varley, T. Lochner and C. Scheu: *J.Power Sources*, Vol. 364 (2017), pp. 437-448
- [5] Mukundan R., Langlois D., Torraco D., Lujan R., Rau K., Spornjak D., Baker A. and Borup R.: *ECS Meeting Abstracts* (2015)

STEAM REFORMING OF BIOETHANOL-GASOLINE MIXTURES

LADENHAUFEN Dominik¹, MALLI Karin¹, HACKER Viktor¹

¹ Graz University of Technology, Institute of Chemical Engineering and Environmental Technology, Inffeldgasse 25/C, 8010 Graz, Austria
d.ladenhaufen@tugraz.at

Keywords: hydrogen production, steam reforming, bioethanol, E85, sulfur

INTRODUCTION

The production of hydrogen via ethanol steam reforming is in an advanced research stage. Ethanol can be produced out of biomass-derived environmental friendly renewable sources like grains, sugar cane, sugar beet or lignocellulose.

Mixing 85 % bioethanol and 15 % gasoline results in the commonly used E85 which is currently available at petrol station in numerous countries. Gasoline might contain sulfur as impurity. This work investigates suitable operating conditions for steam reforming of E85 with and without sulfur.

STEAM REFORMING OF ETHANOL.

Ethanol steam reforming (ESR) can be subdivided into three main reactions: ethanol steam reforming Eq. 1, methane steam reforming Eq. 2 and the water gas shift reaction Eq. 3. The whole reaction process is highly endothermic. Therefore, ESR only takes place at high temperatures.



The whole steam reforming process is complex (seen in Fig.1) and compounds like methane, acetaldehyde and ethylene are common side products [1]. One of the biggest challenges is carbon formation. Among others it is induced by Boudouard reaction, decomposition of methane and polymerisation of ethylene, which lead to deactivation of the catalyst. According to thermodynamics this can be prevented by operating at temperatures above 400 °C and steam to carbon ratios above 1.5.

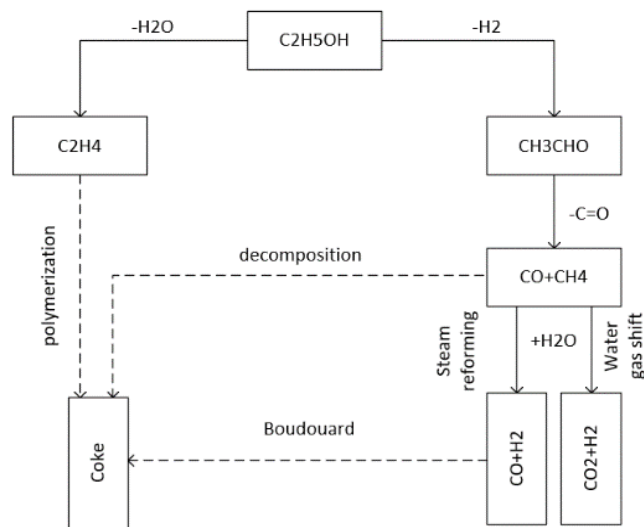


Fig. 3: Reaction pathways [4].

STEAM REFORMING OF SULFUR-FREE E85

E85 is an ethanol – gasoline blend which consists of ethanol (85% anhydrous) and higher hydrocarbons (15% e.g. alkanes, aromatics or alkenes). These additional compounds contribute to the probability of catalyst deactivation caused by carbon deposition. Measures to counteract this type of deactivation are either the increase of temperature or the increase of steam to carbon ratio [2]. As a result, it is important to make a compromise between energy efficiency and stability of the catalyst. This will reduce the catalyst deactivation but will also increase the energy demand of the reforming process. Experiments performed by Simson et al. have shown that steam reforming of this blend could achieve an operation time of 100 hours with an ethanol conversion of over 98% at 650 °C and steam to carbon ratio of 1.8 [3]. Using a Rh/Pt catalyst the product gas consisted of 59 % H₂, 20 % H₂O; 10 % CO; 10% CO₂ and 1% CH₄.

STEAM REFORMING OF E85 WITH SULFUR

Many common transportation fuels contain sulfur. Therefore, E85 usually contains small amounts of sulfur compounds as well. Sulfur is known to have a damaging effect on the catalyst. It increases the formation of coke by increasing the production of acetaldehyde and ethylene. Both are coke precursors and ethylene is one of the most active hydrocarbons to form coke [4]. Even small amounts of sulfur (<5 ppm) increase the formation of coke [3]. To counteract deactivation an increase of temperature and steam to carbon ratio as well as the use of advanced catalysts is necessary. Without this changes the deactivation of the catalyst is dramatic and the conversion of ethanol can drop in a short period of time.

Swartz et al could obtain a good performance over a long period of time using a Rh/ceria catalyst [2]. The dry product gas composition was around 70 % H₂, 20 % CO, 10% CO₂ and 1 % CH₄. This result was only achieved with an increase of the temperature to 800 °C and a high steam to carbon ratio of 6.

CONCLUSION

The steam reforming with E85 is more complex than with pure ethanol. It contains higher hydrocarbons and sulfur, which are serious contributors to catalyst deactivation. Research has shown that the increase of temperature and steam to carbon ratio are necessary to achieve the same results. However, it is important to make a compromise between energy efficiency and stability of the catalyst. It should be considered to remove sulphur before reforming to lower energy input and to increase catalyst durability.

ACKNOWLEDGEMENT

Financial support by the Austrian Federal Ministry of Transport, Innovation and Technology (BMVIT) and The Austrian Research Promotion Agency (FFG) is gratefully acknowledged.

REFERENCES

- [1] H. Xie, E. Weitz, and K. R. Poeppelmeier, "Materials for Clean H₂ Production from Bioethanol Reforming Thermodynamics for Ethanol Steam Reforming (SR) Rh-supported Catalysts," pp. 2–6, 2016.
- [2] S. L. Swartz, P. H. Matter, G. B. Arkenberg, F. H. Holcomb, and N. M. Josefik, "Hydrogen production from E85 fuel with ceria-based catalysts," *J. Power Sources*, vol. 188, no. 2, pp. 515–520, 2009.
- [3] A. Simson, R. Farrauto, and M. Castaldi, "Steam reforming of ethanol/gasoline mixtures: Deactivation, regeneration and stable performance," *Appl. Catal. B Environ.*, vol. 106, no. 3–4, pp. 295–303, 2011.
- [4] A. Simson, S. Crowley, and M. J. Castaldi, "The Impact of Sulfur on Ethanol Steam Reforming," *Catal. Letters*, vol. 146, no. 8, pp. 1361–1372, 2016.

TITANIUM OXIDE NANO-PARTICLES AS SUPPORTS OF CATHODE CATALYSTS FOR POLYMER ELECTROLYTE FUEL CELLS

Yongbing Ma¹, Takaaki Nagai¹, Yoshiro Ohgi², Yoshiyuki Kuroda¹, Koichi Matsuzawa¹, Shigenori Mitsushima^{1,3}, Yan Liu⁴, and Akimitsu Ishihara³

¹ Green Hydrogen Research Center, Yokohama National University, Yokohama, 240-8501, Japan

² Kumamoto Industrial Research Institute, Kumamoto, 862-0901, Japan

³ Institutes of Advanced Sciences, Yokohama National University, Yokohama, 240-8501, Japan

⁴ College of Chemistry and Molecular Engineering, Peking University, Beijing, 10087, China

Keywords: Nb doped TiO₂; Titanium oxide,

INTRODUCTION

Development of carbon-free electro-conductive supports for oxygen reduction catalysts is required for widespread of polymer electrolyte fuel cells because carbon materials used as a support in the present polymer electrolyte fuel cells (PEFCs) are easily oxidized at high potential [1]. Many conductive or semi-conductive oxides have been studied as catalyst support materials or as secondary supports to modify and improve the catalyst support for PEFCs, such as indium tin oxide (ITO) [2], TiO_x [3], SnO₂ [4] and so on. These metal oxides have shown promising effects on the catalytic activity [5,6] and the durability [7,8] of PEFC catalysts. Titanium oxide nanomaterials have been widely used in photocatalysis. Its application as an electrocatalyst support material has also been pursued recently. In addition, Nb-doped TiO₂ shows the high conductivity compare with pure TiO₂, which has the potential that is used as the support.

EXPERIMENTAL

Nb-doped TiO₂ was prepared by hydrothermal method. First, 0.002mol Nb powder and 0.018mol Titanium Butoxide were added in the solution which contained 28% ammonia water and 30% hydrogen peroxide (1:5, v/v), and the dispersion was stirred at room temperature overnight. Then, it was heated at 80 °C, 30 min to vapor NH₃ and H₂O₂, and heated at 180 °C, 20 h to proceed the hydrothermal reaction.

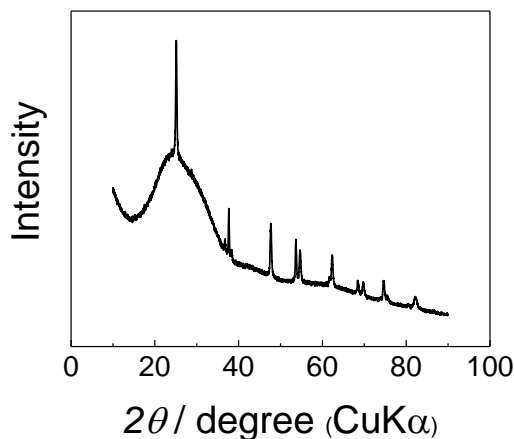


Fig.1 XRD pattern of Nb-doped TiO₂

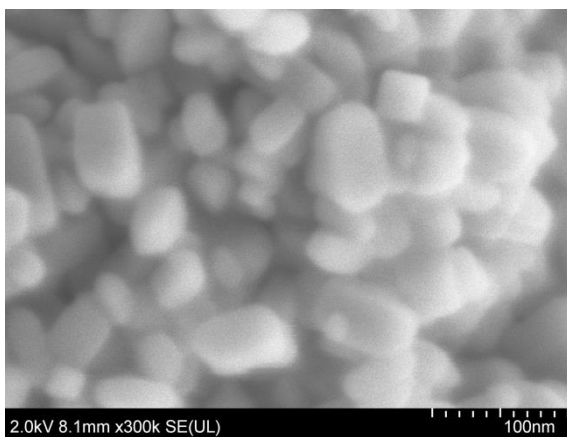


Fig.2 FE-SEM image of Nb-doped TiO₂

Finally, the precipitate was obtained by filtration and dried under vacuum at 100 °C, 6 h. To further improve the conductivity, the Nb-doped TiO₂ particles were reduced at 800 °C under pure hydrogen atmosphere for 1 h.

RESULTS

Fig. 1 shows the XRD pattern of Nb-doped TiO₂ prepared by hydrothermal treatment. According to the XRD pattern, the Nb-doped TiO₂ was identified as the anatase phase. In addition, there were no niobium oxide peaks such as Nb₂O₅. This means that niobium was doped into TiO₂ successfully.

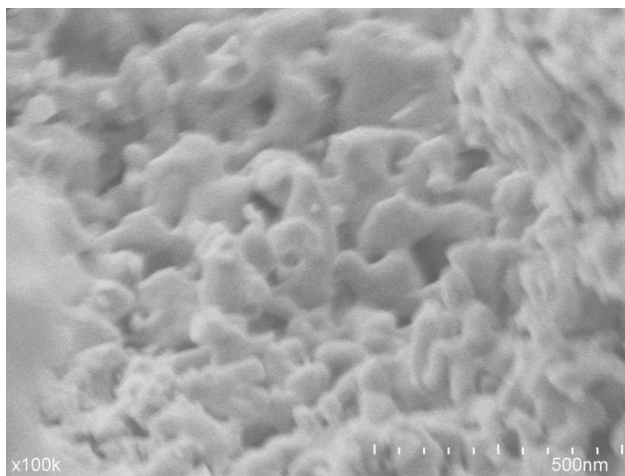


Fig.3 FE-SEM image of Nb-doped TiO₂ after reducing.

Fig. 2 shows the FE-SEM image of Nb-doped TiO₂ particles synthesized by hydrothermal method. The particles are fine which the particle size is approximately 20 nm. The BET surface area was 43 m²g⁻¹.

Fig. 3 shows the FE-SEM image of Nb-doped TiO₂ after reducing. There was some slight melting of the surface of the particles because of the high-temperature treatment of 800 °C. After reducing at 800 °C under pure hydrogen atmosphere for 1 h, the resistivity decreased 14 Ω•cm, which has the potential that is used as the support of the PEFC cathodes.

REFERENCES

- [1] W. Q. Han, et al., *Appl. Phys. Lett.*, 92, 2008, 203117.
- [2] H. Chhina, S. Campbell, and O. Kesler, *J. Power Sources*, 161, 2006, 893–900.
- [3] T. Ioroi, Z. Siroma, N. Fujiwara, S. Yamazaki and K. Yasuda, *Electrochem. Commun.* 7, 2005, 183–188.
- [4] M. S. Saha, R. Y. Li and X. L. Sun, *Electrochem. Commun.*, 9, 2007, 2229–2234.
- [5] H. M. Villullas, F. I. Mattos-Costa and L. O. S. Bulhoes, *J. Phys. Chem. B*, 108, 2004, 12898–12903.
- [6] Z. Jusys, T. J. Schmidt, L. Dubau, K. Lasch, L. Jorissen, J. Garche and R. J. Behm, *J. Power Sources*, 105, 2002, 297–304.
- [7] S. Shanmugam and A. Gedanken, *Small*, 3, 2007, 1189–1193.
- [8] J. A. Tian, G. Q. Sun, L. H. Jiang, S. Y. Yan, Q. Mao and Q. Xin, *Electrochem. Commun.*, 9, 2007, 563–568.

ACKNOWLEDGEMENT

This research was supported by the Strategic International Research Cooperative Program, Japan Science and Technology Agency (JST). This work was conducted under the auspices of the Ministry of Education, Culture, Sports, Science and Technology (MEXT) Program for Promoting the Reform of National Universities.

EXPERIMENTAL SET-UP FOR ETHANOL STEAM REFORMING

Karin Malli¹, Dominik Ladenhaufen¹, and Viktor Hacker¹

¹ Institute of Chemical Engineering and Environmental Technology, Graz University of Technology, Inffeldgasse 25/C, 8010 Graz, Austria
karin.malli@tugraz.at

Keywords: ethanol steam reforming, fuel cells, fuel reforming, gas conditioning

INTRODUCTION

Ethanol is a promising renewable energy carrier for stationary as well as mobile fuel cell (FC) applications. If directly fed to the FC it provides a feasible option to avoid hydrogen infrastructure and storage issues, which still pose a hindrance to full market penetration [1]. Storage and handling of ethanol are comparable to petrol fuel and ethanol production from renewable sources is well established.

In order to directly use carbohydrates with fuel cells it is common practice to combine FCs with a steam reforming unit to provide a hydrogen-rich fuel gas from the carbon source on site [2,3]. The fuel gas either can be directly used in solid oxide fuel cells or must be further treated to meet higher purity standards according to the different types of FCs. This work describes the experimental set-up for the characterization of an ethanol reformer unit for the application with FCs.

THEORETICAL BACKGROUND

Ethanol steam reforming is a catalysed, endothermic process. The overall reaction is described in Equation 1.



In general, the product gas consists of H_2 , CO , CO_2 , CH_4 and H_2O but also side products like acetaldehyde may occur. The composition of the product gas heavily depends on thermodynamics as well as the selectivity and activity of the used catalyst. Fig. 1 shows that a high yield of hydrogen is obtained at high temperatures. Low steam to ethanol ratios are also favourable for obtaining hydrogen-rich synthesis gas. Hence, for fuelling a FC with a reformer, the knowledge of gas composition at the respective operation parameter used is key to a stable operation of the overall system.

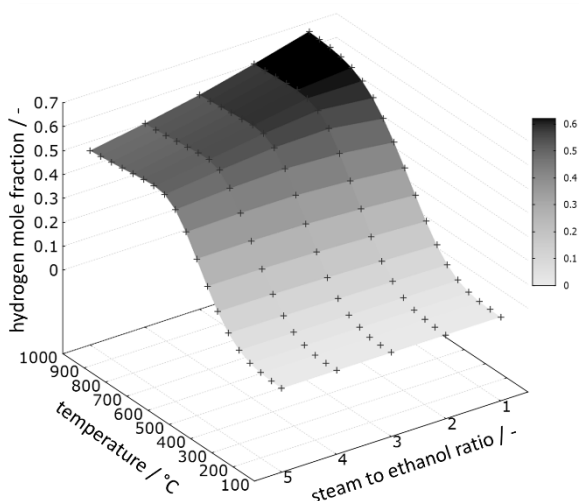


Figure 1: Hydrogen mole fraction of the thermodynamic product composition for steam to ethanol ratios from 1.0 to 5.0 and a temperature range of 100 °C to 1000 °C.

EXPERIMENTAL SET-UP

An overview of the experimental set-up for ethanol steam reforming is shown in Fig. 2. The ethanol steam reaction takes place at the catalyst, which is positioned in the centre of the tube reactor. The reactor itself is heated by a split tube furnace that supplies the catalyst with heat for the endothermic reaction. A gear pump conveys the ethanol-water feed to the system. Before the reactor inlet, the feed stream is heated and vaporized using a direct evaporator. The vapour phase is converted at the catalyst to a hydrogen-rich synthesis gas which mainly consists of H₂, CO, CO₂, CH₄ and H₂O. For analysis, the exiting fuel gas is subsequently separated into a liquid phase and a gas phase through a counter current condenser operating at 4 °C. The gas stream is analysed online with a gas chromatograph (GC; microGC 3000, inficon). In this set-up the total product gas stream is determined with an internal standard, which is added to the feed before the reactor inlet. A GC (GC-2010-Plus, Shimadzu) is used to analyse the condensate for remaining ethanol and other organic compounds, which may occur as side products of the catalytic reaction.

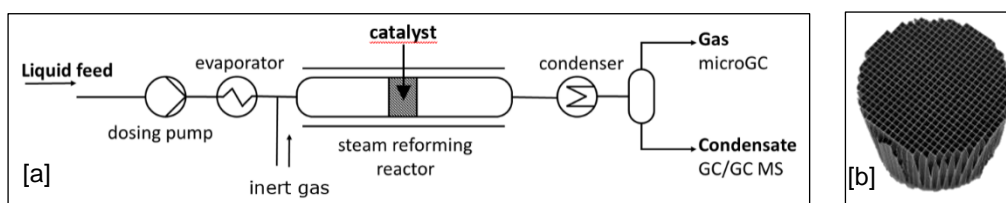


Figure 2: [a] Shows an overview of an experimental set-up for ethanol steam reforming. [b] Shows a common monolithic honeycomb catalyst used for steam reforming.

By using these analytical methods, the fuel gas stream composition can be characterized in detail. The data provide important information about catalytic selectivity, activity and the deactivation behaviour, which are needed for a reliable operation of a reformer - fuel cell system.

ACKNOWLEDGEMENT

Financial support by the Austrian Federal Ministry of Transport, Innovation and Technology (BMVIT) and The Austrian Research Promotion Agency (FFG) is gratefully acknowledged.

REFERENCES

- [1] J.W. Kim, K.J. Boo, J.H. Cho, I. Moon, Key challenges in the development of an infrastructure for hydrogen production, delivery, storage and use, in: A. Basile, A. Iulianelli (Eds.), *Adv. Hydrog. Prod. Storage Distrib.*, Woodhead P, Woodhead Publishing, 2014: pp. 3–31.
- [2] H. Ito, Economic and environmental assessment of residential micro combined heat and power system application in Japan, *Int. J. Hydrogen Energy*. 41 (2016) 15111–15123. doi:10.1016/j.ijhydene.2016.06.099.
- [3] M. Prigent, On Board Hydrogen Generation for Fuel Cell Powered Electric Cars. A Review of Various Available Techniques, *Rev. l'Institut Français Du Pétrole*. 52 (1997) 349–360. doi:10.2516/ogst:1997045.

STRUCTURE DEPENDENCE OF OER ACTIVITY IN POROUS NICKEL ELECTRODE

Haruki Masumura¹, Yoshiyuki Kuroda¹, Kouichi Matsuzawa¹, Takahiro Higashino², Kazuki Okuno², Hiromasa Tawarayama², Masatoshi Majima², and Shigenori Mitsushima¹

¹ Graduated School of Engineering Science, Yokohama National University, 79-5 Tokiwadai, Hodogaya-ku, Yokohama 240-8501, Japan

² Energy and Electronics Materials Laboratory, Sumitomo Electric Industries, Ltd., 4-5-33 Kitahama, Chuo-ku, Osaka 541-0041, Japan

E-mail: cel@ml.ynu.ac.jp

Keywords: alkaline water electrolysis, oxygen evolution reaction, porous Ni

INTRODUCTION

Alkaline water electrolysis (AWE) have some advantages, such as low cost and large scale production of H₂, whereas voltage loss is relatively large. It is expected that the voltage loss decreases by using porous electrode with large surface area. However, in gas evolution reaction, much pore walls of porous electrode are electrochemically inactive as they are covered with gas bubbles [1]. Here, we investigated the effect of porous structure on voltage loss of AWE anode from the viewpoint of effective surface area and mass transport, using macroporous Ni with a Raney Ni layer on the surface.

EXPERIMENTAL

Four porous or nonporous Ni electrodes were used in this study. Celmet[®] provided by Sumitomo Electric Industries, Ltd. was used as a microporous material. A Raney-Ni was used as a microporous material which was prepared by dealloying NiZn alloy plated on a Ni plate. Hierarchically porous material with both macro- and micropores was prepared by dealloying of NiZn alloy plated on a Celmet[®]. Ni_{plate} was treated in 25wt% HNO₃ at 90°C for 6 min. NiZn_{plate} and NiZn_{porous} were heated in Ar at 380°C for 1h, followed by etching in 7 M KOH at 100°C for 1h. The electrodes were characterized by scanning electron microscopy (SEM) and inductively coupled plasma optical emission spectroscopy (ICP-OES).

Electrochemical measurements were performed in a three-electrode cell with the porous Ni electrodes and a Ni_{plate} as a working electrode, Ni coil as a counter electrode and RHE as a reference electrode (All potentials were shown vs. RHE.). The electrolyte was 7M KOH at 30°C. For electrochemical pretreatment, Cyclic voltammetry (CV) was performed for 100 cycles from 0.05 to 1.5 V (all electrodes), 20 cycles (Ni_{plate}, Ni_{porous}), or 30 cycles (NiZn_{plate}, NiZn_{porous}) from 1.0 to 1.5 V with the scan rate of 50 mV s⁻¹. The following techniques were used for analyzing electrode performances.

CV from 0.5 to 1.5 V with the scan rate of 5 mV s⁻¹ for 5 cycles. Chrono amperometry (CA) at given potentials for 600 s. The potentials were 1.5–2.2 V (Ni_{plate}, Ni_{porous}), or 1.6– 1.8 V (NiZn_{porous}, NiZn_{plate}). Electrochemical impedance spectroscopy (EIS) was measured with at 1.5–1.85 V (Ni_{plate}, Ni_{porous}) or, 1.5–1.7 V (NiZn_{porous}, NiZn_{plate}). The frequency range was 10⁻¹ to 10⁵ Hz and the amplitude was 10 mV.

RESULTS AND DISCUSSION

The effect of macropore was investigated using Ni_plate and Ni_porous. Figure. 1 shows the electric double layer capacitance (C_{dl}) at various steady state current densities ($t = 600$ s, $i_{@600s}$). The capacitance of both Ni_plate and Ni_porous decreased greatly at $i_{@600s} = 10$ mA cm⁻² and they were almost constant value at $i_{@600s} > 50$ mA cm⁻². Generated bubbles might block macropore surfaces during the OER reaction. Although the specific surface areas of Ni_porous_0.45 and Ni_porous_0.8 were 16 and 7 times larger than that of Ni_plate respectively, the C_{dl} values were only 1.5 and 1.2 times respectively. Ni_porous_0.8 with larger pore size showed relatively large effective surface area than Ni_porous_0.45, suggesting facile removal of gas bubbles from larger pores.

Figs. -2, and -3 show the polarization curves of porous Ni electrodes obtained by CV. Current densities in Fig. 2 and Fig. 3 are normalized by geometric surface area (i_{geo}), and C_{dl} (i) respectively. NiZn_plate and NiZn_porous with micropores showed much larger current densities normalized by geometric surface area, though the values were below those of Ni_porous and Ni_plate when the values were normalized by C_{dl} . C_{dl} reflects electrochemical active surface area. Therefore, these results indicate that electrochemical active area are not fully used in microporous Ni electrodes. In the literatures, reporting hydrogen evolution from Raney-Ni electrode [2], the utilization of micropores was small because of the high concentration of dissolved H₂ due to capillary force in micropores. In conclusions, the introduction of macro- and microporous structure to Ni electrode is effective to improve OER activity. However, the activity was smaller than those predicted by the geometrical surface areas because of bubbles and capillary effects.

REFERENCE

- [1] S. Rausch, H. Wendt, J. Electrochem. Soc., 143, 2852 (1996)
- [2] S. Rausch et al., J. Appl. Electrochem., 22, 1025 (1992)

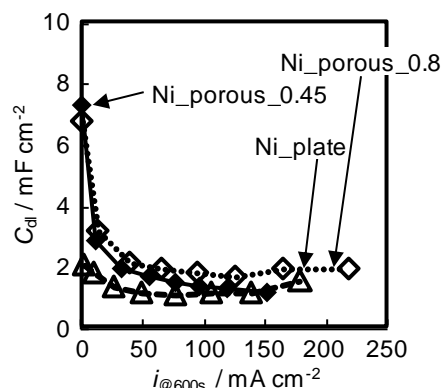


Fig. 1 Electric double layer capacitance (C_{dl}) of Ni_porous and Ni_plate from EIS as a function of current density at $t = 600$ s ($i_{@600s}$) measured by CA.

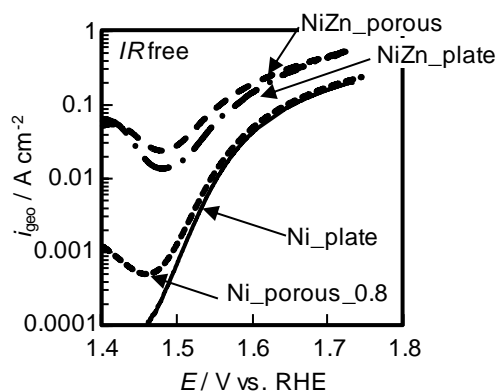


Fig. 2 Polarization curves of porous Ni electrode from SSV. Current density is normalized by geometric surface area.

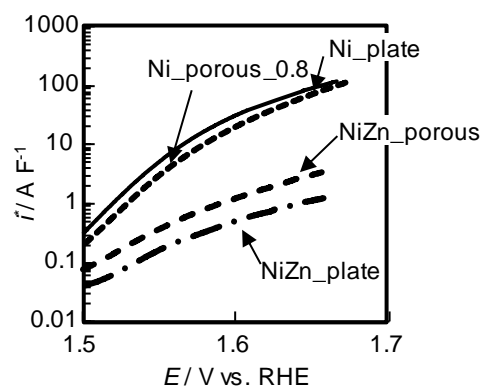


Fig. 3 Polarization curves of porous Ni electrode from CV. Current density is normalized by double layer capacitance.

PERMEABILITY OF TOLUENE AND METHYLCYCLOHEXANE FOR PROTON EXCHANGE MEMBRANE

Takehiro Misu¹, Kensaku Nagasawa², Yoshiyuki Kuroda¹, Koichi Matsuzawa¹, and Shigenori Mitsushima^{1,2}

¹ Green Hydrogen Research Center, Yokohama National University, 79-5 Tokiwadai, Hodogaya-ku, Yokohama 240-8501, Japan

² Institute of Advanced Sciences, Yokohama National University, 79-5 Tokiwadai, Hodogaya-ku, Yokohama 240-8501, Japan

E-mail: cel@ml.ynu.ac.jp

Keywords: proton exchange membrane, toluene, methylcyclohexane, hydrogenation

INTRODUCTION

Hydrogen has been expected as the clean energy carrier, which is synthesized using renewable energies. However, the hydrogen energy carrier has been needed, because the long distance and the large-scale transportation of gas state at ambient temperature is inefficiency. The toluene / methylcyclohexane organic chemical hydride system is one of the candidates of a hydrogen energy career. This system is easy to handle due to the liquid state at ambient temperature. We have been focused on the one-step hydrogenation reaction from toluene to methylcyclohexane with water decomposition. This method has higher conversion efficiency than conventional two-step reaction of the water electrolysis and the hydrogenation, because the one-step reaction can prevent the exothermic heat loss and decrease the theoretical decomposition voltage [1]. For the toluene hydrogenation electrolyzer, the permeation of toluene through ionomer in cathode catalyst layer affect to mass transport resistance of cathode, and simultaneously from cathode to anode through the proton exchange membrane (PEM) leads the degradation of the anode [2]. However, kinetics of the toluene permeability for PEMs has not been known well. In this study, we have been evaluated toluene and methylcyclohexane permeability and investigated the permeability as a function of operation-temperature.

EXPERIMENTAL

Nafion[®] membrane (N117: thickness $d = 183 \mu\text{m}$) were used as PEM. As pretreatment, PEM was immersed in 1.0 M ($=\text{mol dm}^{-3}$) sulfuric acid for 2 h. 1.0 M sulfuric acid and 100% toluene(TL₁₀₀) or 50% toluene(TL₅₀)/50% methylcyclohexane(MCH) were separated with the PEM in a cell. The toluene and methylcyclohexane amounts which permeated to the sulfuric acid thorough PEM were measured by a gas chromatography (GC). A small amount of the sulfuric acid that contained toluene and methylcyclohexane was sampled into n-hexane to extract toluene and methylcyclohexane from aqueous solution in temperature range from 25 to 60°C. Solubility of toluene or methylcyclohexane in sulfuric acid was also measured with GC analysis of aqueous phase of mixture of toluene or methylcyclohexane and sulfuric acid using a separating funnel.

RESULTS AND DISCUSSION

The permeated toluene concentration as a function of time: $C(t)$ was represented as the following equation with linear concentration profile of toluene and methylcyclohexane to thickness direction in a membrane.

$$C(t) = C_{\max}\{1-\exp(-SDHt/Vd)\} \quad (1)$$

where, S , D , H , t , V , and d are permeation area, diffusion coefficient of toluene or methylcyclohexane, distribution coefficient of toluene or methylcyclohexane at sulfuric acid-PEM interface, time, volume of sulfuric acid, and thickness of PEM, respectively. The C_{\max} is the solubility of toluene or methylcyclohexane in sulfuric acid. The apparent diffusion coefficient of toluene or methylcyclohexane in PEM, which defined as the product of diffusion coefficient and distribution coefficient ($= DH$), was determined from the $C(t)$ and C_{\max} using the eq. (1).

Figure 1 shows the concentration of toluene and methylcyclohexane as a function of time at 60°C. The lines were fitted by the function to the eq. (1). The order of permeated concentrations was $MCH < TL_{50} < TL_{100}$. This order corresponded with the order of each saturation concentration. Although the transmission density varies depending on the saturation concentration, TL_{100} , TL_{50} , and MCH can be explained by linear concentration diffusion because they can be fitted by the eq. (1).

Figure 2 shows the Arrhenius plot for apparent diffusion coefficient of toluene and methylcyclohexane. Both DH s of TL_{50} and TL_{100} were close to each other, the apparent transmittances were the positive dependence on the rise of temperature. This result showed that the permeation mechanism of toluene did not change even in the presence of methylcyclohexane. The apparent activation energies of TL (TL_{50} , TL_{100}) and MCH were about 23 kJ mol^{-1} and 16 kJ mol^{-1} , respectively. These values were close to 18 kJ mol^{-1} of methanol [3] and larger than 9.6 kJ mol^{-1} of proton [4]. Protons in the membrane are permeated by both the Grotthuss mechanism, which moves by proton exchange between water molecules, and the Vehicular mechanism, which migrates as the move of hydronium ion. Toluene, methylcyclohexane and methanol permeate by only the Vehicular mechanism. Hence, these activation energies would be higher than proton.

ACKNOWLEDGEMENTS

This work was supported by Toyota Mobility Foundation. The Institute of Advanced Sciences (IAS) in YNU is supported by the MEXT program for Promoting Reform of National Universities. We appreciate the person concerned them.

REFERENCES

- [1] K. Nagasawa, Y. Sawaguchi, A. Kato, Y. Nishiki, and S. Mitsushima, *Electrocatalysis*, 8, 164–169 (2017).
- [2] K. Nagai, K. Nagasawa, and S. Mitsushima, *Electrocatalysis*, 7, 441–444 (2016).
- [3] V. Tricoli, et al., *Journal of Electrochemical Society*, 147, 4, 1286-1290 (2000)
- [4] M. A. Hickner, C. H. Fujimoto, and C. J. Cornelius, *Polymer*, 47, 4238-4244 (2006).

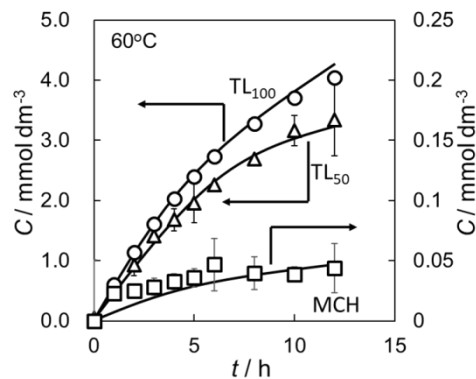


Fig. 1. Permeated concentration of toluene and methylcyclohexane in the sulfuric acid through the N117 as a function of time at 60°C

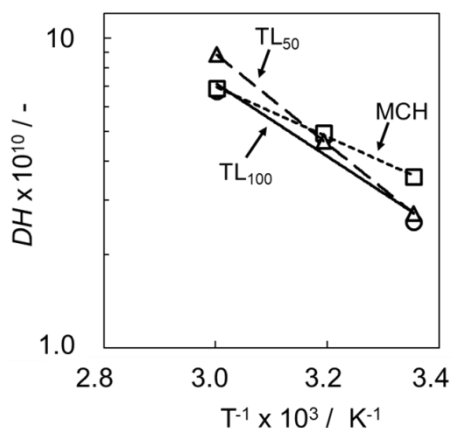


Fig. 2. Arrhenius plot for apparent diffusion coefficient of toluene and methylcyclohexane

TOTAL HARMONIC DISTORTION ANALYSIS OF FLOODING AND DRY OUT IN SIMULATIONS AND EXPERIMENTS

Kurt Mayer¹, Viktor Hacker¹

¹ Institute of Chemical Engineering and Environmental Technologies (CEET), Fuel Cell Systems Group, Graz University of Technology, Inffeldgasse 25C, 8010 Graz, kurt.mayer@tugraz.at

Keywords: PEMFC, flooding, dryout, electrochemical impedance spectroscopy (EIS), total harmonic distortion analysis (THDA), small (dynamic large) signal equivalent circuits (S-/DLSEC), simulation.

INTRODUCTION

Confronted with the threat of climate change, greenhouse gases have to be decreased by introducing more renewable energy sources. Especially in the mobile sector, one of such technologies is the polymer electrolyte membrane fuel cell (PEMFC). Advantages of the initiation of fuel cells are the absence of greenhouse gas emissions, the high energy conversion efficiency and its high power density. However, two of the biggest drawbacks are the high costs and the low lifetime that prevent fuel cell operated cars from being commercially available on large scale up to now.

This paper will concentrate on total harmonic distortion analysis (THDA) at normal operating conditions, flooding and dry out. This technique is non-invasive, can be deployed during operation and is a fast and easy way to detect and identify faulty operating conditions which are responsible for the low lifetime.

EXPERIMENTAL AND SIMULATIONS

Experimental. A PEMFC stack consisting out of 5 fuel cells with an active surface area of 50 cm² is obtained from ZBT (Duisburg). The mass flow of hydrogen is 1.2 l h⁻¹ with a stoichiometry of 1.5 on the anode side, on the cathode side synthetic air with a mass flow of 3 l h⁻¹ and a stoichiometry of 2.5 is provided. All experiments are obtained under ambient pressure. While recording impedance spectra at different operating points, the temperature of the stack is kept constant and the THD values are recorded by the hardware as well. After each measurement series the temperature of both humidifiers is changed in 10 °C steps from 50 °C to 80 °C. EIS measurements are executed by imposing an alternating current (AC) signal (amplitude: 500 mA, frequency range: 10 kHz to 100 mHz) on a direct current (DC) with the power potentiostat PP240 by Zahner Elektrik.

Simulations. The simulation software is described by Weinberger et al. [1]. In general, the small signal equivalent circuit (SSEC) is extended to a dynamic large signal equivalent circuit (DLSEC) by replacing the charge transfer resistor, R_{ct} , and the concentration resistance, R_{conc} , with current controlled voltage sources providing the charge transfer overpotential and the concentration overpotential, respectively. With the fitted DLSEC parameters from the impedance spectra, the DLSEC can be used for THD simulations.

RESULTS AND DISCUSSION

In Figure 1a the experimental THD data of the fuel cell stack, operated at dry out conditions (temperature of stack: 70 °C, relative humidity of gases: 35.2%rH, operating point: 0.3 A cm⁻²), is plotted against the frequency. At very low excitation frequencies (below 1 Hz) peaks in THD spectra can be detected. Figures 1b and 1c present the simulated FFT spectra of the output

voltage signal at the same operating conditions, if the stack is excited with a sinusoidal input signal with a frequency of 0.5 Hz and 1 Hz, respectively. As can be seen, more harmonics arise at 0.5 Hz which results in a higher THD at 0.5 Hz than at 1 Hz. Together with the experimental result, this indicates that dry out can be detected if the stack is excited below 1 Hz.

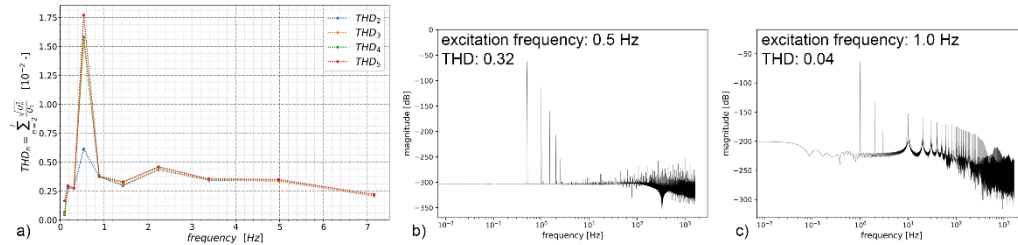


Figure 1: (a) experimental THD spectrum at dryout; FFT spectra of output voltage signal at excitation frequency of (b) 0.5 Hz and (c) 1 Hz.

Looking at Figure 2a, the experimental THD spectrum at flooding conditions (temperature of stack: 70 °C, temperature of humidifiers: 80 °C, operating point: 0.3 A cm²) can be seen. THD spectra of flooding conditions exhibit peaks at excitation frequencies above and equal to 1.5 Hz. Figure 2b and 2c show again the simulated FFT spectra of the output voltage signal at the same operating conditions and at excitation frequencies of 0.5 Hz and 1.5 Hz, respectively. This time more harmonics can be observed at 1.5 Hz excitation frequency. Again, these simulation results together with the experimental data support the thesis that flooding can be detected at excitation frequencies above and equal to 1.5 Hz.

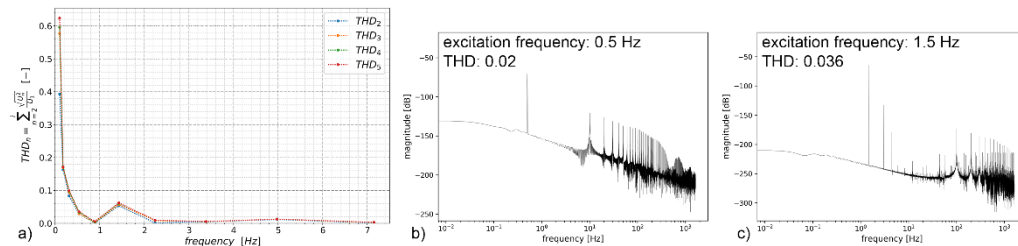


Figure 2: (a) experimental THD spectrum at flooding; FFT spectra of output voltage signal at excitation frequency of (b) 0.5 Hz and (c) 1 Hz.

CONCLUSION

Experimental THD spectra as well as simulated FFT spectra of the output voltage signal show that in certain excitation frequency ranges peaks can be detected, that allow the identification of and differentiation between faulty operating conditions. Dryout can be detected below an excitation frequency of 1 Hz, flooding above 1.5 Hz. The experimental THD values are much higher than the simulated ones. On the one hand, noise of experimental data can result in higher harmonic content. On the other hand, the harmonic content during parameterization of the EIS spectra is neglected which also decreases the THD values of simulation results.

ACKNOWLEDGEMENTS

This work is funded by the Austrian Ministry of Transport, Innovation and Technology (BMVIT), the Austrian Research Promotion Agency (FFG) and the International Energy Agency (IEA).

REFERENCES

- [1] Weinberger S, Trattner S, Cermek B, Schenk A, Grimmer C, Hacker V: J Energy Storage 2017;12:319–31.

FCEV SYSTEM AND DRIVELINE SIMULATION ANALYSIS BY USING AVL CRUISE M

Juergen Rechberger¹, Farzaneh Moradi¹, and Alireza Moradi²

¹ AVL List GmbH, Graz, Austria

² Shiraz Islamic Azad University, Shiraz, Iran

Global concerns on sustainable energy use and environmental protection call for innovative powertrain technologies. Among the alternative powertrains, Fuel Cell Electric Vehicles (FCEVs) incorporating hybrid powertrains with electric energy supplied by a fuel cell and / or by a battery are considered as a viable solution allowing for long driving range and short fueling time thereby offering similar driving experience as vehicles powered by internal combustion engines (ICEVs). Development of such complex systems as FCEVs crucially relies on the application of modelling and simulation tools. They allow for a cost and time efficient identification of the most promising solutions, and therefore support frontloading in the development process yielding reduced development effort and costs. To comply with these objectives and to efficiently support the virtual development process, a powerful, robust and adaptable tool that supports everyday tasks in vehicle system and driveline simulation analysis is required.

AVL CRUISE M is a realtime, multi-disciplinary, vehicle system simulation software used in office environments for the design of powertrains and thermal management systems, in HiL environments for control function development and calibration, and in testbed environments to provide simulation models for component testing. AVL CRUISE M offers a streamlined workflow for all kinds of parameter optimization and component matching. Using AVL CRUISE M the performance of a FCEV (e-motor: 85 kW, battery capacity: 8.8 kWh, fuel cell power: 50 kW, vehicle curb weight: 1614 kg) was simulated. In order to calculate the hydrogen consumption and the vehicle driving range, three driving cycles including: NEDC, WLTC and GRDE were simulated. Table 1 shows the results of these simulations.

Moreover, gradeability simulations were also performed. The vehicle was tested under two different slopes (8 and 16%). The simulation results for these two slopes illustrate that the vehicle is able to maintain a constant speed of 55 km/h and 85 km/h without battery supply and a speed of 90 km/h and 135 km/h with battery supply for 16% and 8% slopes respectively.

Furthermore, full load acceleration and elasticity simulations were run with and without battery support. The results of these simulation are presented in Table 2.

An additional simulation was performed to determine vehicle's top speed on flat road. The outcome was a top speed of 140 km/h, where the gear ratio limits the reachable top speed.

Table 1: Simulated H₂ consumption and driving range for three different cycles

Cycle	H ₂ consumption (kg/100 km)	Estimated total driving range (km)*
NEDC	0.88	~427
WLTC	1.03	~366
GRDE	1.17	~316

Table 2: Simulated full load acceleration and elasticity

Simulated parameter	Power source	Time (s)
Full load acceleration 0-100 kph	With battery	12.1
	Without battery	22.7
Elasticity 80-120 kph	With battery	10.1
	Without battery	23.8

REFERENCES

- [1] Dj. M. Maric, P.F. Meier and S.K. Estreicher: Mater. Sci. Forum Vol. 83-87 (1992), p. 119
- [2] M.A. Green: High Efficiency Silicon Solar Cells (Trans Tech Publications, Switzerland 1987).
- [3] Y. Mishina, in: Diffusion Processes in Advanced Technological Materials, edited by D. Gupta Noyes Publications/William Andrew Publishing, Norwich, NY (2004), in press.
- [4] G. Henkelman, G. Johannesson and H. Jónsson, in: Theoretical Methods in Condensed Phase Chemistry, edited by S.D. Schwartz, volume 5 of Progress in Theoretical Chemistry and Physics, chapter, 10, Kluwer Academic Publishers (2000).
- [5] R.J. Ong, J.T. Dawley and P.G. Clem: submitted to Journal of Materials Research (2003)
- [6] P.G. Clem, M. Rodriguez, J.A. Voigt and C.S. Ashley, U.S. Patent 6,231,666. (2001)
- [7] Information on <http://www.weld.labs.gov.cn>

MODEL ELECTRODE OF OXYGEN REDUCTION CATALYST FOR PEFCs BASED ON ZIRCONIUM OXIDE BY ARC PLASMA DEPOSITION

K. Nagano¹, A. Ishihara², T. Nagai¹, Y. Kuroda¹, K. Matsuzawa¹, S. Mitsushima^{1,2} and K. Ota¹

¹ Green Hydrogen Research Center, Yokohama National University, 79-5 Tokiwadai, Hodogaya-ku, Yokohama, 240-8501, Japan, cel2@ml.ynu.ac.jp

² Institute of Advanced Sciences, Yokohama National University, 79-5 Tokiwadai, Hodogaya-ku, Yokohama, 240-8501, Japan, cel2@ml.ynu.ac.jp

Keywords: Polymer electrolyte fuel cells, Oxygen reduction reaction, Oxide-based cathode, Zirconium oxide

INTRODUCTION

Because Polymer Electrolyte Fuel Cells (PEFCs) have high theoretical energy conversion efficiency, practical use as power sources for stationary residential cogeneration system and fuel cell vehicles has already been started. In the present PEFC, platinum nano-particles on carbon support are used as an oxygen reduction catalyst. However, platinum is expensive and has small resources. In addition, the durability of carbon support is insufficient at high potential. In order to widely commercialize PEFCs, the development of an alternative material as non-platinum cathode is inevitable. In this study, we focused on zirconium oxide for alternative material. Because zirconium oxide-based powder catalysts with some oxygen reduction reaction (ORR) activity show a large resistivity, it is difficult to form a sufficient electron conduction path without the existence of the other electro-conductive materials such as carbon. Therefore, it is necessary to evaluate the size and/or the thickness of the zirconium oxide-based catalysts whose surface could act as active sites although the catalysts have poor conductivity.

EXPERIMENTAL

We prepared model catalysts using an arc plasma deposition (APD) method. Metal Zr was used as a target, and oxygen pressure in chamber was controlled to form ZrO_{2-x} . Fig. 1. shows an image of APD. By changing the number of shots of arc plasma, we could control easily the average film thickness of zirconium oxide on glassy carbon (GC) plate and investigate the effect on the ORR activity. We used three-electrode cell for electrochemical measurements. The electrolyte was 0.1 mol dm^{-3} sulfuric acid and the temperature was kept at 30 ± 0.5 °C. The reference electrode was a reversible hydrogen electrode (RHE), and the counter electrode was a GC plate. Cyclic voltammetry was performed in nitrogen atmosphere with a scan rate of 150 mV s^{-1} . The potential was scanned between $0.2 \text{ V} - 1.1 \text{ V}$ vs. RHE in oxygen or nitrogen atmosphere with a scan rate of 10 mV s^{-1} to obtain the ORR current. The ORR activity was evaluated by the oxygen reduction current density based on geometric area (i_{ORR}).

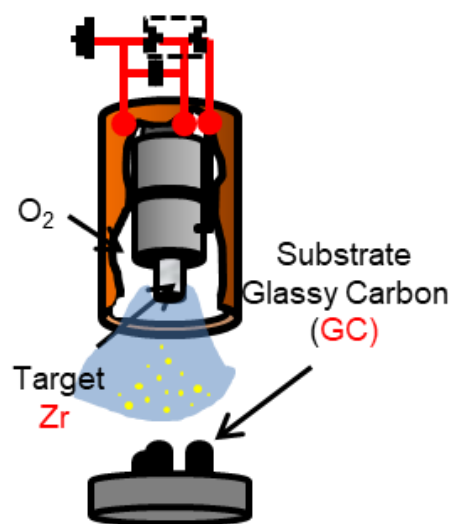


Fig. 1. Image of APD

RESULTS AND DISCUSSION

Fig. 2 shows the dependence of the electric double layer capacitance (C) obtained from the cyclic voltammograms on the average film thickness. C was increased until the average film thickness of ca. 1 nm, and decreased with increasing the film thickness. It is well known that the quantum tunneling of electrons through the insulator film occurs when the thickness of the insulator is below a few nanometers. The increase in C below the 1 nm indicated that the surface of the zirconium oxide in the region electrochemically activated due to the quantum tunneling of electrons. When the thickness of the zirconium oxide increased above 2 nm, it was difficult to occur the quantum tunneling of electrons because the zirconium oxide films were almost insulators.

Fig. 3 shows the relationship between the average film thickness of ZrO_{2-x} and the i_{ORR} at 0.3 V. The i_{ORR} increased with increasing the average film thickness of 1 nm, and gradually decreased. This result suggested that the surface of the zirconium oxide nanoparticles and/or film prepared by APD had active sites for the ORR.

Therefore, we found that when the particle size or the thickness of the zirconium oxide could be prepared to be 1 nm or less, all of its surface would be electrochemically activated and show the ORR activity even in the powder catalyst. This finding gives the important information in the catalyst design and preparation of oxide catalysts with poor conductivity.

ACKNOWLEDGEMENTS

The authors thank New Energy and Industrial Technology Organization (NEDO) for financial support. This work was also supported by the Izumi Science and Technology Foundation, Tonen General Sekiyu Research / Development Encouragement & Scholarship Foundation, and JSPS KAKENHI Grant Number JP18K05291. This work was conducted under the auspices of the Ministry of Education, Culture, Sports, Science and Technology (MEXT) Program for Promoting the Reform of National Universities.

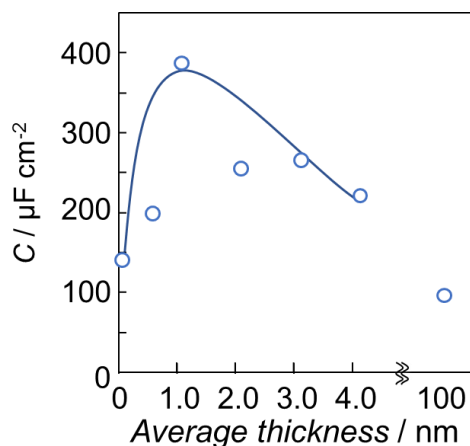


Fig. 2. Dependence of electric double layer capacitance of ZrO_{2-x} -based catalysts prepared by APD on average film thickness.

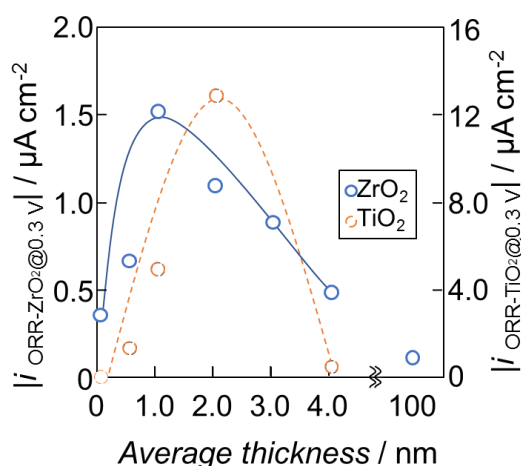


Fig. 3. Relationship between average film thickness and oxygen reduction current density at 0.3 V.

ELECTRICAL EFFICIENCY AND THERMAL AUTONOMY OF POWER GENERATION SYSTEM USING PROTONIC CERAMIC FUEL CELL

Takeshi Nakayama¹, Toshiki Kawamura², and Takuto Araki³

¹ Graduate School of Engineering, Yokohama National University, Japan, nakayama-takeshi-hx@ynu.jp

² Graduate School of Engineering, Yokohama National University, Japan, kawamura-toshiki-dh@ynu.jp

³ Faculty of Engineering, Yokohama National University, Japan, taraki@ynu.ac.jp

Keywords: Protonic ceramic fuel Cell (PCFC), Efficiency of power generation system

INTRODUCTION

In order to improve the electrical efficiency of a SOFC (solid oxide fuel cell), operating under the high fuel utilization rate is one method. However, in the case of using oxide-ion-conducting SOFC under high utilization rate, not only the fuel is diluted with the produced vapor, but also Ni contained in the electrode material is oxidized because reduction can not be maintained[1]. On the other hand, in the case of using protonic ceramic fuel cell(PCFC), since the generation of steam accompanying power generation occurs on the air electrode side, fuel dilution does not occur and operation at a high fuel utilization rate is possible. Furthermore, the proton conducting electrolyte maintains a high ionic conductivity in the medium temperature range (500 to 700°C), so that the cost of peripheral equipment can be reduced. The system calculation (Matuzaki et al. [2]) shows that it is theoretically possible to maintain the high fuel utilization rate and achieve high electrical efficiency exceeding 80% based on the lower heating value (LHV). In this study, efficiency calculation of power generation system using PCFC and thermal autonomy of the system were investigated. Furthermore, heat loss was estimated by assuming the dimensions of the SOFC stack and the hot zone and improvement of electrical efficiency was also studied.

RESEARCH METHODS

Fig.1 shows the system. The power generation system consisted of heat exchangers, combustor, reformer, SOFC stack, and air blower. Thermodynamic calculation and chemical equilibrium calculation based on heat/material balance calculations were performed for each element. Calculation conditions at that time were set based on Solid Power's BlueGEN standard, the AC output was 1.5 kW and the electrical efficiency was 63.0% (AC, LHV). In addition, the evaluation of thermal autonomy was examined from the possibility of establishment of heat exchangers when heat loss was added to the system. Temperature efficiency, which is an index of heat exchanger performance, was set at 90% to the upper limit in consideration of size and cost. Thermal autonomy means that heat generation accompanying power generation and heat generation in the combustor of unused fuel can cover the necessary amount of heat for the entire system, and the supply of heat from the outside is not necessary.

RESULT AND DISCUSSIONS

Fig. 2 shows a result of temperature efficiency vs. heat loss. Temperature efficiency is a parameter that shows performance of heat exchanger. Temperature efficiency less than 90% was set as a condition that the thermal autonomy of system can be maintained. By system calculation, it was shown that total heat loss can be tolerated up to 350W in order to maintain thermal autonomy. However, it is difficult to completely insulate. The heat loss from the hot zone to the

surroundings was expected to be about 100W even when using a stack with high power density ($3\text{W}/\text{cm}^3$) or a high performance heat insulating material (thermal conductivity $0.04\text{W}/\text{m K}$). Therefore, the remaining 250W after subtracting the hot zone heat loss from the allowable heat loss can be expected to improve the electrical efficiency. In that case, it is suggested that the electrical efficiency improves to about 73.5% (AC, LHV).

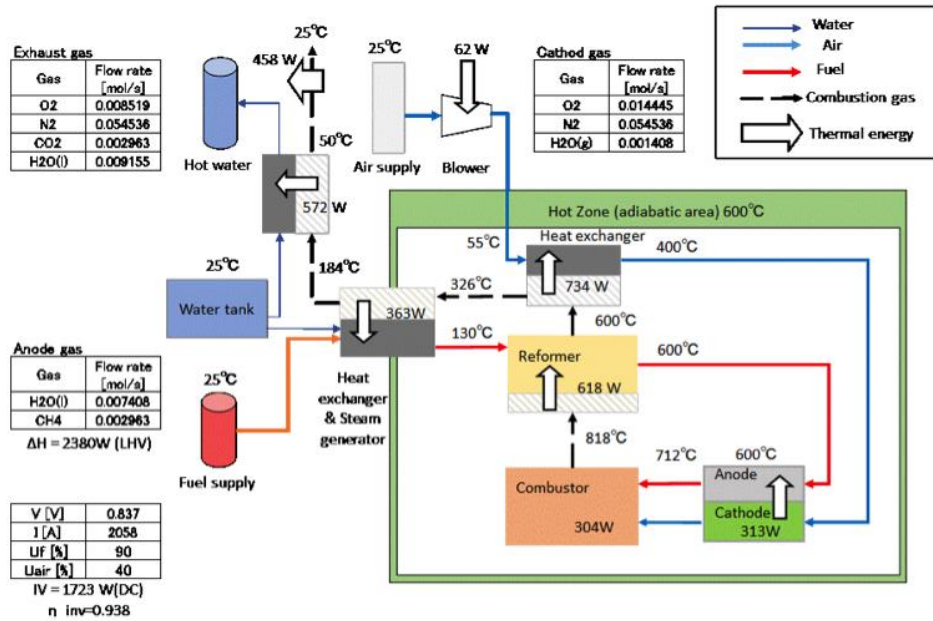


Fig.1 System model at AC 1.5kW export power

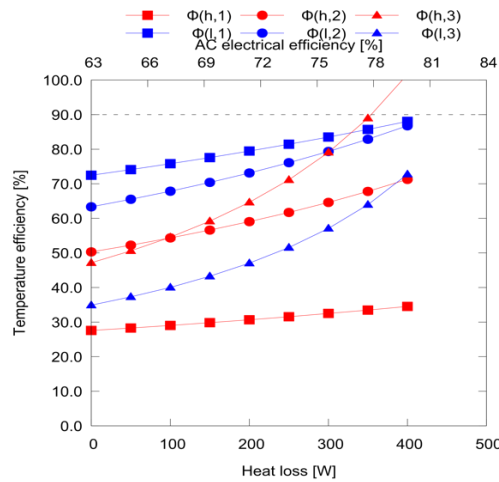


Fig.2 Temperature efficiency vs. heat loss and AC electrical efficiency at AC 1.5kW export power

REFERENCES

- [1] S. Lee, H. Kim, K. J. Yoon, J.-W. Son, J.-H. Lee, B.-K. Kim, W. Choi and J. Hong, International Journal of Heat and Mass Transfer, 97, 77–93 (2016).
- [2] Y. Matsuzaki, Y. Tachikawa, T. Somekawa, T. Hatae, H. Matsumoto, S. Taniguchi and K. Sasaki, Scientific Reports, 5(1), 12640 (2015).

ACTIVITY OF Pt-Pd CATALYSTS SUPPORTED ON CARBON BLACK TOWARDS OXYGEN REDUCTION REACTION

Linathi Ndzuzo¹, Juan Carlos Calderón Gomez, Sivakumar apsupathi.

¹ South African Institute of Advanced Material Chemistry, Private Bag X17, Bellville, 7535, Cape Town, South Africa, 3341694@myuwc.ac.za

Keywords: Carbon blacks, oxygen reduction reaction, Pt-Pd catalyst.

INTRODUCTION

Proton exchange membrane fuel cells (PEMFCs) are electrochemical device that convert the chemical energy from a fuel into electricity through an electrochemical reaction between hydrogen and oxygen. It is developed for transport, stationary and portable applications. Their high efficiency and cleanness of PEMFCs attract a lot of interest from researchers in the last years [1]. In the cathode of the PEMFC takes place the oxygen reduction reaction characterised by its sluggish kinetics through two pathway mechanisms such as the production of water involving four electrons and the production of hydrogen peroxide implying two electrons [2]. An important issue with PEMFC is the lack of alternative catalysts to platinum for the oxygen reduction reaction (ORR). The high cost and limited availability of platinum restricts its long term use for large scale applications and commercialisation of PEMFC. Consequently, there is a great interest in alternative catalysts to platinum for PEMFC such as metal alloys. In this study, platinum alloyed with palladium catalysts supported on carbon black were synthesised in order to evaluate their activity towards oxygen reduction reaction. There were five synthesis routes used employing five different reducing agents which include propanol, ethanol, methanol, ascorbic acid and formaldehyde respectively. The synthesis methods had a planned composition of metal content close to 40 wt. % and Pt:Pd atomic ratios around 1:2. The prepared Pt-Pd/CB catalysts were physically characterised by EDS, XRD and TEM in order to determine their composition and physical and morphological properties. The catalytic activity towards oxygen reduction reaction was assessed by electrochemical techniques such as rotating-disk electrode (RDE) and cyclic voltammetry (CV) as shown in figure 1. All synthesized Pt-Pd/CB catalysts showed an improved diffusion current density when compared to the commercial Pt/C catalyst. The Pt-Pd/CB-AA and Pt-Pd/CB-nPrOH showed the most improvement with diffusion current densities close to -5.8 and -5.3mA cm² respectively compared to the commercial Pt/C catalysts which showed -4.3mA cm².

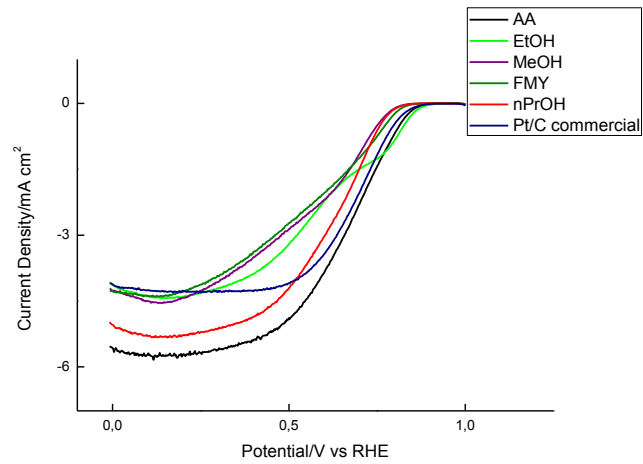


Figure 1: RDE measurements of synthesized Pt-Pd/CB and Pt/C commercial catalysts at 1600rpm in O₂ saturated 0.1M HClO₄ at scan rate of 2m.V⁻¹.

REFERENCES

- [1] Zhi-Min, Z; Zhi-Gang, S and Xiao-Ping, Q. Durability study of Pt-Pd/C as PEMFC cathode catalyst. International Journal of Hydrogen Energy, 2010, 35, 1719-1726.
- [2] Gasteiger, H.A; Kocha, S.S; Sompalli, B; and Wagner, F.T. Activity benchmarks and requirements for Pt, Pt-alloy, and non-Pt oxygen reduction catalysts for PEMFCs, Applied Catalysis, B: Environmental, 2005, 56, 9-35

TEMPERATURE MEASUREMENT USING THIN FILM THERMOCOUPLE DURING PEFC COLD START

Yota OTSUKI¹, Yusuke TAMADA², and Takuto ARAKI³

¹ Graduate School of Eng., Yokohama National University, Japan, otsuki-yota-xj@ynu.jp

² Graduate School of Eng., Yokohama National University, Japan, tamada-yusuke-nt@ynu.jp

³ Faculty of Eng., Yokohama National University, Japan, taraki@ynu.ac.jp

Keywords: Cold start, Thin Film Thermocouple, Micro Electro Mechanical Systems

INTRODUCTION

Polymer electrolyte fuel cell (PEFC) is attracting attention as a clean and highly efficient power generation system. However, problems caused by start-up in a subzero environment remain to be solved. It is considered that moisture generated by the reaction exists in the battery as a supercooled state or ice in subzero environment. Y. Ishikawa et al. [1] reported that when they observed the moisture generated on the CL surface using a transparent cell, the produced water did not freeze quickly and maintained the supercooled state. On the other hand, small ice formed inside the battery gradually grows and interferes with the supply of the reaction gas and becomes a cause of performance deterioration. Eventually it causes shutdown. Therefore, it is important to understand the mechanism of ice formation and supercooled water freezing within PEFC at the time of subzero start.

We have developed thin film thermocouples using MEMS technology to measure the temperature inside the PEFC directly. In this report, we focus on the heat generated when the supercooled water is frozen and report the temperature change in the cell in a form closer to the real machine by using this thin film thermocouple.

EXPERIMENTAL METHOD

Fig. 1 shows a schematic diagram of the experiment and Fig. 2 shows the configuration of the cell used in the measurement.

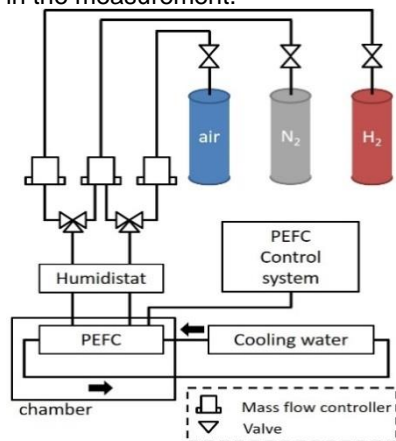


Fig. 1 Schematic view of experimental system

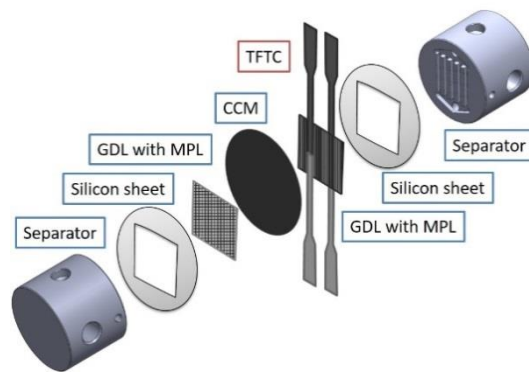


Fig. 2 The configuration of PEFC cell

The PEFC cell configuration is formed by putting Catalyst coated membrane (CCM) between Micro porous layer (MPL), Gas diffusion layer (GDL), silicone sheets and separators. Separators were made of graphite, reaction area 1 cm², parallel flow channel shape with rib width and channel width of 1 mm respectively. The thin-film thermocouple was inserted so as to be positioned on rib one by one at the CCM/MPL and GDL/separator interface.

Previous work has reported that the residual moisture inside the cell influences the starting characteristics when cold start-up is performed [2]. In conducting the measurement, purging was carried out with a humidified nitrogen gas after the break-in process. After the purge was completed, the cell was cooled. Table 1 shows the details of the experimental conditions.

MEASUREMENT RESULTS

Fig. 3 (a) shows the cell voltage, the separator temperature of the anode and the cathode, and the measured temperature of the CL/MPL interface and the GDL/separator interface from the start-up to the shutdown. The reason why the cell temperature and the temperature of the thin film thermocouple insertion part are not stable during operation is that the cooling temperature itself is unstable. This instability is due to the temperature accuracy of the constant temperature bath (LTB - 125, AS ONE) that is cooling. Voltage drop began around 600 seconds after start of operation, and operation stopped after another 200 seconds. In addition, instantaneous temperature rise is observed at both the CL/MPL interface and the GDL/separator interface at the moment when the cell voltage drop begins. This temperature rise is thought to be the heat of solidification generated when the moisture freezes from the supercooled state. Fig. 5 (b) shows a graph enlarging the time domain at this moment. An instantaneous temperature rise can be confirmed.

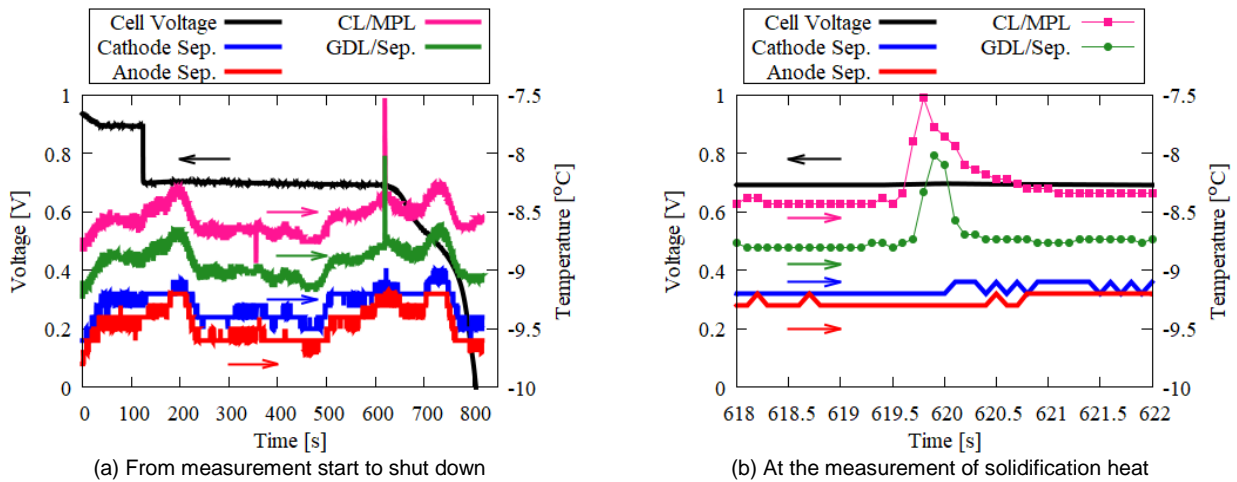


Fig. 3 Measured voltage and temperature during PEFC cold start

REFERENCES

- [1] Y. Ishikawa et al., Super-cooled water behavior inside polymer electrolyte fuel cell cross-section below freezing temperature, *Journal of Power Sources*, 179(2008), pp. 547-552.
- [2] K. Tajiri et al., Water removal from PEFC during gas purge, *Electrochimica Acta*, 53(2008), pp. 6337-6343.

MANUFACTURE AND OPERATION OF 60 cm² ZINC-AIR FLOW BATTERIES WITH BIFUNCTIONAL AIR ELECTRODES

Birgit PICHLER¹, Hans-Jürgen Pauling², Viktor HACKER¹

¹ Institute of Chemical Engineering and Environmental Technology,
Graz University of Technology,
Inffeldgasse 25/C/II, 8010 Graz, Austria
birgit.pichler@tugraz.at

² RECAT GmbH, Ochsenburger Str. 19, 75056 Sulzfeld Germany

Keywords: Zinc/air, flow batteries, air electrodes, bifunctional catalyst, pulse charging

INTRODUCTION

The Zinc-air flow battery is considered to be a promising technology for large-scale electrical energy storage due to the use of inexpensive, abundant and non-toxic active material zinc and the compact system design with only one storage tank and without a membrane [1]. The energy efficiency of the system is mainly determined by the oxygen catalysis on the air electrode, *i.e.* oxygen reduction reaction (ORR) during discharge and oxygen evolution reaction (OER) during charge. Perovskite oxide catalysts are a low-cost alternative to noble-metal catalysts and exhibit good bifunctional activity and stability during cycling. In this work, La_{0.6}Sr_{0.4}Co_{0.2}Fe_{0.8}O₃ perovskite was implemented in stable 60 cm² electrodes and these electrodes optimized for long-term cycling operation [1-4].

EXPERIMENTAL

Commercially acquired La_{0.6}Sr_{0.4}Co_{0.2}Fe_{0.8}O₃ perovskite was homogenously dispersed on carbon nanofibers, and mixed with PTFE as hydrophobic binder material (paste 1) and additionally with nickel powder in paste 2. Each paste was spread on opposite sides of nickel foam, dried and press-sintered at 150 kg cm⁻² and 300 °C (Fig.1 right).

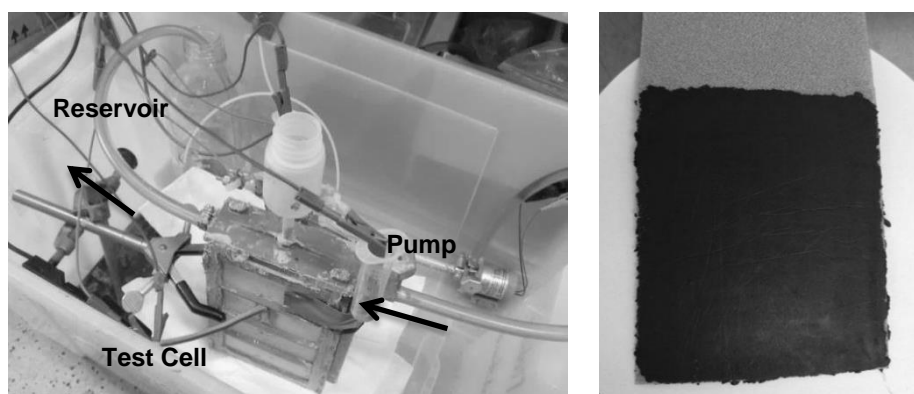


Fig. 1: Image of the flow battery test set-up with 1 L reservoir and modular test cell for up to 100 cm² sized electrodes (left) and image of the 60 cm² sized bifunctional air electrode before sintering.

Galvanostatic cycling (pulse charge/1 h discharge) via the air electrode was performed with a BaSyTec potentiostat in a full cell set-up using a zinc plate as negative electrode in 8 M KOH + 0.5 M ZnO electrolyte at 25 °C (Fig.1 left). The flow rate was about 2 cm s⁻¹.

RESULTS AND DISCUSSION

As shown in Fig.2, the tested air electrode (black) exhibited stable charge/discharge potentials over the course of 300 h and 100 cycles. Within the first 50 h of testing significant improvement of ORR and OER performance is apparent through the decreasing potential difference ΔV between charge and discharge. At 50 mA cm^{-2} the ORR potential was approximately $0.8 \text{ V vs. Zn/Zn}^{2+}$ and the corresponding charge potential about 2.1 V . The pulse charging (black bars) did not negatively influence the stability of the air electrode [3,4]. The difference between air electrode potentials and cell voltage (grey) resulted from the overpotentials of the zinc electrode and ohmic losses from the electrolyte. After 300 h of testing, the cell potential dropped at the end of each discharge cycle due to deteriorating zinc electrode reversibility. Nevertheless, short circuits, usually caused by zinc dendrite formation, were prevented by the pulse charging.

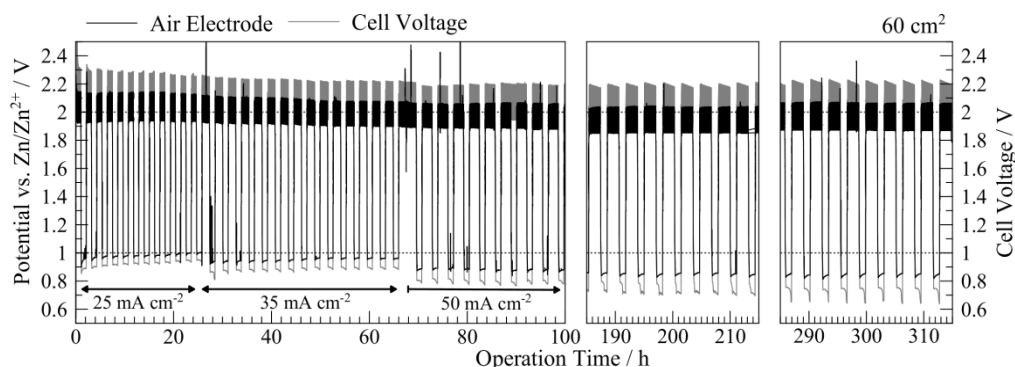


Fig. 2: Long-term cycling (100 cycles) of a 60 cm^2 bifunctional air electrode (black) and the corresponding cell potential (grey) at $25 - 50 \text{ mA cm}^{-2}$ discharge with 50 mA cm^{-2} pulses ($50 \text{ ms} + 50 \text{ ms}$ no current) during pulse charging ($1 - 2 \text{ h}$ charging).

OUTLOOK

Further improvement of the discharge performance of the air electrode is needed in order to raise the voltage efficiency of the cell to $>50\%$, which can be achieved by balancing the hydrophobicity within the electrode. In addition, shape change of the whole zinc electrode needs to be prevented, for example by deposition of zinc on copper foam current collector.

ACKNOWLEDGEMENT

Funding of this project by the Austrian Research Promotion Agency (FFG) and the Climate and Energy Fund through the program "Energieforschungsprogramm 2015" (no. 848933) is gratefully acknowledged.

REFERENCES

- [1] J. Fu, Z.P. Cano, M.G. Park, A. Yu, M. Fowler, Z. Chen, Electrically Rechargeable Zinc-Air Batteries: Progress, Challenges, and Perspectives, *Adv. Mater.* 29 (2017)
- [2] B. Pichler, S. Weinberger, L. Reščec, V. Hacker, Development of Stable Bifunctional Air Electrodes for Zinc-Air Flow Batteries, *ECS Trans.* 80 (2017) 371–375.
- [3] B. Pichler, S. Weinberger, L. Reščec, I. Grimmer, F. Gebetsroither, B. Bitschnau, V. Hacker, Bifunctional electrode performance for zinc-air flow cells with pulse charging, *Electrochim. Acta.* 251 (2017) 488–497.
- [4] B. Pichler, B. Berner, N. Rauch, C. Zelger, H.-J. Pauling, B. Gollas, V. Hacker, Component and electrode development of zinc-air flow batteries at varying operating conditions, *J. Appl. Electrochem.* (accepted)

EFFECTS OF THE EXISTENCE OF MPL AND GDL POROSITY TO THE LOCAL TEMPERATURE AND WATER DISTRIBUTION IN PEFC

Kaito SHIGEMASA¹, Yusuke TAMADA², Sota HASHIMURA³ and Takuto ARAKI⁴

¹ Graduate School of Engineering, Yokohama National University, Japan, shigemasa-kaito-mp@ynu.jp

² Graduate School of Engineering, Yokohama National University, Japan, tamada-yusuke-nt@ynu.jp,

³ Graduate School of Engineering, Yokohama National University, Japan, hashimura-souta-bv@ynu.jp

⁴ Faculty of Engineering, Yokohama National University, Japan, taraki@ynu.jp

Keywords: PEFC, X-ray, Thin-film thermocouple, heat conductivity.

INTRODUCTION

Fuel cells are attracting attention as clean energy. There are some kinds of fuel cells, and among them, polymer electrolyte fuel cells (PEFC) has higher power density than other fuel cells and has been partially put into practical use, such as fuel cell vehicles, because of its low operating temperature. However, there are many problems and one of the most important tasks is the management of the temperature inside the PEFC. Then in this study, we used X-ray CT to visualize the liquid water in the PEFC, and thin-film thermocouple (TFTC) to measure inside the cell during operating. From these results, it was investigated how Gas Diffusion Layer (GDL) properties influence the interrelationship between liquid water distribution in PEFC and temperature difference between top and bottom of the GDL.

EXPERIMENT

Cell configuration

The PEFC cell we used is made from resin impregnated graphite so that we can focus on only water distribution inside cathode GDL. We used 3 GDLs made by SIGRACET to research the effect with the existence of MPL and porosity of GDL, and the type numbers are SGL28BC, SGL29BC, and SGL29BA. The typical material data of GDLs are shown as Table 1. Micro Porous Layer (MPL) is a layer which is on the GDL to raise drainage of GDL.

Table 1 Typical material data of GDL

Parameters	Units	SGL28BC	SGL29BC	SGL29BA
Thickness	μm	235	235	200
Porosity	%	82	88	88
Thermal conductivity	W/(mK)	0.6	0.5	0.4-0.5
MPL	-	with	with	without

Thin-film thermocouple (TFTC)

We used TFTC to measure local temperature inside PEFC. TFTC should be as thin as possible to keep TFTC from inhibiting the reaction inside PEFC. Therefore, TFTC with the thickness of about

9 μm were fabricated using MEMS technology. We have to calibrate for each sensor because each sensor has different Seebeck coefficient. We have inserted TFTC into the interface between Catalyst Layer (CL) and GDL and measured local temperature there.

X-ray CT

We used the X-ray CT to visualize water distribution inside PEFC. The visualization conditions are that the tube voltage is 30 [kV], tube current is 200 [μA] and the number of view is 3600/180 $^\circ$ [-]. Moreover, the voxel size of the image is about 2.7 [μm] and it takes about 15 [min] to get cell image from CT machine.

Operation conditions

We set the cell temperature 60 [$^\circ\text{C}$], the gas of anode H_2 , the gas of cathode Air, the gas flow rates of anode 1000 [mL/min], cathode 1000[mL/min] and relative humidity of the gas 40 [%] or 100 [%], which are the same as both side

RESULTS AND DISCUSSION

Figure 1 shows the arithmetic average value of the temperature increase from the separator temperature on the cathode side and the calorific value obtained by the thin film thermocouple when we used SGL 29 BC and SGL 28 BC and relative humidity of the supply gas was 40 [%]. The horizontal axis means current density [A/cm^2] and the vertical axis means temperature increase [$^\circ\text{C}$]. The temperature increase of 0 [A] was set to 0 [$^\circ\text{C}$] to focus on only temperature increase. Fig.1 shows that the more porosity GDL has, the more temperature difference there is inside PEFC. Figure 2 shows brightness distribution of the cell image. The horizontal axis means how far from CCM and the vertical axis means brightness. In the cell image, the less amount of X-ray which achieves to the camera is, the higher brightness of the image is. Therefore, we can evaluate how much water there is inside PEFC by evaluating how high the brightness is. We have to pay attention that the reason the brightness around 0 pixel is higher is there is Platinum of CL. Fig.2 shows when we used SGL29BC, the amount of water in the cathode GDL was changed at 1.0 [A], but when we used SGL28BC, the water amount was changed at 0.4 [A]. Therefore, that may mean there are some difference how water fills in cathode GDL by the difference of the porosity.

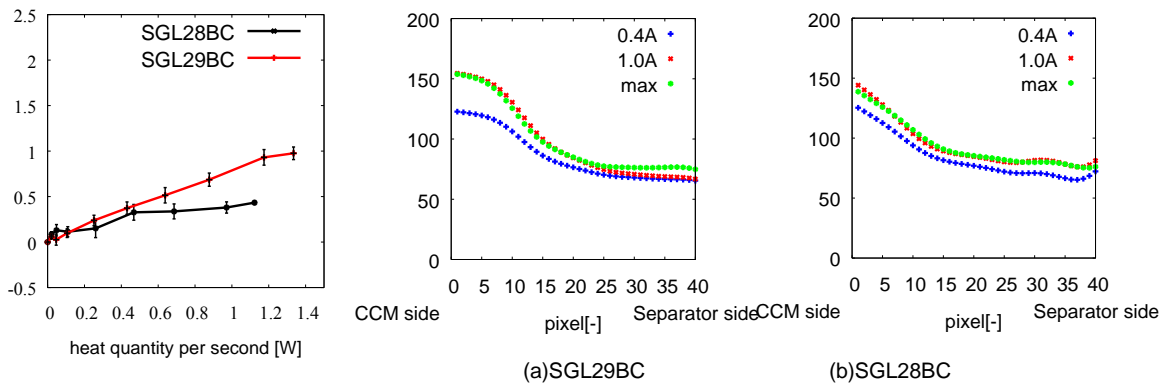


Fig.1 Temperature increase

Fig.2 Brightness distribution

Interrelationship between local temperature and water distribution

In Fig.2(a), we can see the brightness increase at max current density and in Fig.2(b), at 1.0A. Moreover, in Fig.1, the gradient of temperature increase changed between 0.4 [A] and 1.0[A] in SGL28BC and changed around max current density in SGL29BC. This may mean the state of heat transfer was changed by water in cathode GDL. We think thermal resistance of cathode GDL was lowered by water and the gradient of temperature increase decreased.

EFFECT OF FORMATION OF ELECTRON CONDUCTION PATH ON ZIRCONIA SURFACE ON OXYGEN REDUCTION ACTIVITY

Wataru Shimabukuro¹, Akimitsu Ishihara², Takaaki Nagai¹, Yoshiyuki Kuroda¹, Koichi Matsuzawa¹, Shigenori Mitsushima^{1,2} and Ken-ichiro Ota¹

¹ Green Hydrogen Research Center, Yokohama National University, 79-5 Tokiwadai, Hodogaya-ku, Yokohama, 240-8501 JAPAN, cel2@ml.ynu.ac.jp,

² Institute of Advanced Sciences, Yokohama National University, 79-5 Tokiwadai, Hodogaya-ku, Yokohama, 240-8501 JAPAN, cel2@ml.ynu.ac.jp

Keywords: Polymer electrolyte fuel cell (PEFC), Oxygen reduction reaction (ORR), Powder catalysts, Non-platinum catalysts, Group 4 and 5 metal oxides.

INTRODUCTION

Polymer electrolyte fuel cell (PEFC) have already been commercialized in Japan as power supply of fuel cell vehicles and residential use. At present, platinum supported carbon black (Pt/C) is used as a cathode catalyst of PEFC. Pt has a lot of problems such as low resources, high cost, dissolution and precipitation during operation for a long time to decrease the cell performance. We focused on group 4 and 5 metal oxides as non-platinum cathodes for PEFC, because their oxides have some merits such as low cost, abundant resources, and high stability in acidic media. We found that the oxygen vacancies formed on the surface of oxides or the distortion in the crystal structure acted as an active site of the ORR [1]. We believe that when the group 4 and 5 metal oxides can substitute for Pt/C catalysts, PEFC can be commercialized widely. However, group 4 and 5 metal oxides are generally insulators with a large band-gap. Therefore, even if metal oxides have adsorption sites of oxygen molecules which can become active sites for the ORR, the oxygen reduction current doesn't flow because of lack of formation of electron conduction path, resulting that it is difficult to evaluate the ORR activity appropriately. In this research, we investigated the evaluation method to evaluate the ORR activity of metal oxides and examined the heat-treatment conditions for higher ORR activity. At first, in order to obtain the sufficient conductivity from outside to oxide surface, carbon powder was mixed with the oxide powder by ball-milling. In addition, we carried out reductive heat-treatment of ball-milled powder catalysts to obtain higher ORR activity.

EXPERIMENTAL

ZrO₂ powder (TECNAN, Particle size: 10 nm) and carbon powder (Cup Stack Carbon Nano-Tube: CSCNT, GSI Creos) were mixed by a planetary ball mill with a weight ratio of oxide and carbon was 2 : 8. Rotation speed was 560 rpm and holding time was 180 min. Material of ball and container was Cr steel and the atmosphere in the container was Ar. For comparison, only CSCNT powder was ball-milled under the same condition, and another sample mixed with oxide and carbon was also prepared by Auto Mortar for 1h. The sample prepared by ball-milling was heat-treated under reductive atmosphere such as at 600 °C for 10 min under 4%H₂.

A 1-Hexanol and 5wt% Nafion[®] added to the obtained powder catalysts, and a catalyst ink was prepared after ultrasonic dispersion. The ink was dropped on the glassy carbon (GC) rod. The GC rod loaded catalyst was used as a working electrode. A three-electrode cell was used for the electrochemical measurements. The electrolyte was 0.1M H₂SO₄ at 30 °C, and a reference electrode was a reversible hydrogen electrode (RHE), and a counter electrode was a GC plate. As a pretreatment, cyclic voltammetry (150 mV sec⁻¹, 0.05 - 1.2 V vs. RHE, 300 cycles) was carried

out in an oxygen atmosphere. Next, cyclic voltammetry (50 mV sec^{-1} , $0.05 - 1.2 \text{ V}$, 10 cycles.) was carried out in a nitrogen atmosphere. Double layer capacitance was calculated from the current at the range from 0.8 to 1.0 V . Slow scan voltammetry (5 mV sec^{-1} , $0.2 - 1.2 \text{ V}$, 4 cycles) was carried out in an oxygen atmosphere or in a nitrogen atmosphere, respectively. The current at 4 cycle during a cathodic sweep was subtracted, and the subtracted value was taken as the oxygen reduction current (i_{ORR}).

The notation of catalyst is expressed as {carbon support name / oxide name_detailed condition}.

RESULTS AND DISCUSSION

Figs.1 and 2 show the cyclic voltammograms (CVs) and the ORR polarization curves of samples with different mixing methods and a sample with reductive heat-treatment at $600 \text{ }^\circ\text{C}$. {CSCNT / ZrO_2 _Ball Mill} has larger double layer capacitance and higher ORR activity than {CSCNT / ZrO_2 _Auto Mortar}, indicating that the electron conduction path was effectively formed by ball-milling. The CV and the i_{ORR} of a sample containing ZrO_2 were larger than those of only carbon with ball-milling. This difference was attributed to oxides. According to these results, the ORR activity essentially derived from ZrO_2 is easier to observe when carbon is mixed with the oxide using ball-milling.

In addition, the ORR activity was improved by reductive heat-treatment. Although the lattice distortion of the crystalline structure and the formation of oxygen vacancies would effect the ORR activity, we need to investigate the effect in future.

CONCLUSION

The mixture of ZrO_2 and CSCNT prepared by ball-milling had larger CV and higher ORR activity than that prepared by auto-mortar. This reason was considered that the electron conduction path was effectively formed by ball-milling. In addition, the samples with reductive heat-treatment showed higher ORR activity, indicating that the lattice distortion of the crystalline structure and the formation of oxygen vacancies would enhance the ORR activity.

ACKNOWLEDGEMENT

The authors thank New Energy and Industrial Technology Organization (NEDO) for financial support. This work was supported by the Izumi Science and Technology Foundation, Tonen General Sekiyu Research / Development Encouragement & Scholarship Foundation, and JSPS KAKENHI Grant Number JP18K05291 and conducted under the auspices of the Ministry of Education, Culture, Sports, Science and Technology (MEXT) Program for Promoting the Reform of National Universities.

REFERENCES

- [1] A. Ishihara, M. Tamura, Y. Ohgi, M. Matsumoto, K. Matsuzawa, S. Mitsushima, H. Imai, and K. Ota, J. Phys. Chem. C, 117, 18837 (2013)

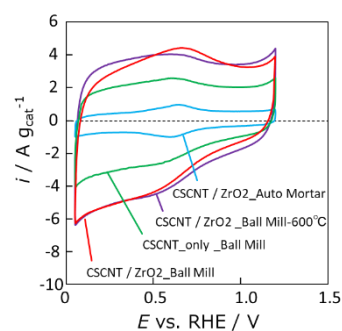


Fig1. CVs of catalysts.

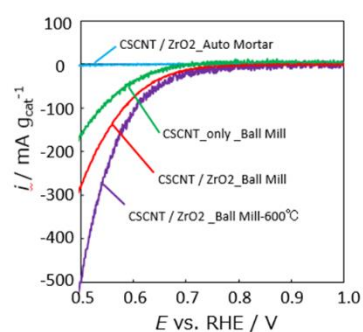


Fig2. i_{ORR} of catalysts.

STUDY OF OXYGEN EVOLUTION REACTION ON ZIRCONIUM OXIDE-BASED MODEL ELECTRODE

Kyogo Sumi¹, Koichi Matsuzawa¹, Yoshiyuki Kuroda¹, Akimitsu Ishihara², Shigenori Mitsushima^{1,2} and Ken-ichiro Ota¹

¹ Green Hydrogen Research Center, Yokohama National University, 79-5 Tokiwadai, Hodogaya-ku, Yokohama 240-8501, Japan, sumi-kyogo-ph@ynu.jp

² Institute of Advanced Sciences, Yokohama National University, 79-5 Tokiwadai, Hodogaya-ku, Yokohama 240-8501, Japan, ishihara-akimitsu-nh@ynu.ac.jp

Keywords: Oxygen Evolution Reaction, Zirconium Oxide, Thin Film Catalyst, Arc Plasma Deposition Method

INTRODUCTION

The oxygen electrode reaction is important for hydrogen production and utilization devices such as water electrolysis and fuel cell. In addition, this reaction is also applied for the metal-air batteries. For installation of these electrochemical devices on a large scale, the inexpensive electrode with high stability and activity for oxygen evolution reaction (OER) should be required [1]. Because of its high stability, we have focused on 4 and 5 group oxide, especially on the zirconium oxide. We have applied it for the OER electrocatalyst [2]. In this study, the OER activity of Zr oxide thin film catalyst on 0.5 atm% Nb-doped TiO₂ plate has investigated. The Zr oxide thin film catalyst was prepared by arc plasma deposition (APD) method.

EXPERIMENTAL METHODS

(1) Preparation of Model Electrode

Nb 0.5 atm% doped TiO₂ rutile (110) single crystal (12×12 mm) plate was used as substrate. Thermal treatment was carried out at 600°C for 150 min. Thin film catalyst was prepared by APD method with the capacitance condition of 1080 μF [3]. The pulse voltage was 100 V and film deposition rate was 0.061 nm / Pulse. A film thickness controlled by the number of pulse.

(2) Electrochemical Measurement

The electrochemical property was measured by three-electrode cell. As the reference, counter, and working electrodes, RHE, a glassy carbon plate, and zirconium oxide thin film on 0.5 atm% Nb-doped TiO₂ rutile (110) single crystal (ZrO_x / Nb doped TiO₂) were used, respectively. The measurement was carried out in 7 M KOH at 30±1°C. The double layer capacitance (C_{dl}) was evaluated by cyclic voltammetry with scan rate of 50 mV s⁻¹ in 0.05-1.2 V vs. RHE, and then the OER activity was evaluated by slow scan voltammetry with scan rate of 5 mV s⁻¹ in the range of 1.0-1.7 V vs. RHE. The film resistance (R_{film}) was determined by the electrochemical impedance spectroscopy (EIS) in the range of 1.5-1.7 V with an amplitude of 10 or 50 mV in the frequency range of 0.1~100 kHz.

RESULTS AND DISCUSSION

Fig. 1 shows the Dependence of C_{dl} and R_{film} on film thickness of ZrO_x . The C_{dl} was calculated from dividing by scan rate the average of geometric current density (i_{geo}) in 0.8-1.0 V. The C_{dl} was decreased with the increase of film thickness and finally reached to $0.60 \mu F cm^{-2}$ in the film thickness of 50 nm. In contrast, the R_{film} was increased with the film thickness and finally reached to $13 k\Omega cm^{-2}$ in the film thickness of 50 nm while it was $0.55 k\Omega cm^{-2}$ in the case of the film thickness of 0.5 nm.

Fig. 2 shows Tafel plots of ZrO_x / Nb doped TiO_2 . Tafel slope of Zr oxide catalysts were $53-73 mV dec^{-1}$ while that of the substrate was $190 mV dec^{-1}$. The onset potential of OER was defined as the electrode potential at $0.3 \mu A cm^{-2}$ of i_{geo} . The average of OER onset potential of ZrO_x was $1.49 V$ vs. RHE, while that of substrate was $1.59 V$. Compared to the OER activity of substrate, it reveals that the OER activities of ZrO_x thin film were improved.

In order to compare the OER activity and film thickness ZrO_x , the i_{geo} at $1.56 V$ in the Tafel region was used as an index of OER activity. Fig. 3 shows the dependence of OER activities on the thickness of ZrO_x film. As a result, the OER activity was dependent on the thickness of ZrO_x film. The ZrO_x film with thickness of 10 nm had $5.47 \mu A cm^{-2}$ of i_{geo} and the highest OER activity in this study.

REFERENCES

- [1] A. Ishihara, Y. Ohgi, K. Matsuzawa, S. Mitsushima and K. Ota: *Electrochim. Acta* Vol. 55 (2010), p. 8005
- [2] A. Oishi, K. Matsuzawa, Y. Kohno, A. Ishihara, S. Mitsushima, Proc. 39th Meeting of Electrolytic Technol. Jpn (2015) p. 86 (in Japanese)
- [3] Y. Agawa, E. Sakae, A. Saito, K. Yamaguchi, M. Matsuura, K. Suzuki, Y. Hara, M. Nakano, N. Tsukahara, Y. Murakami: *Ulvac Tech. J.* Vol. 65 (2006), p. 1

ACKNOWLEDGEMENTS

This work was supported by Toyota Mobility Foundation. The Institute of Advanced Sciences (IAS) in YNU is supported by the MEXT Program for Promoting the Reform of National Universities. We appreciate the assistance of the person concerned.

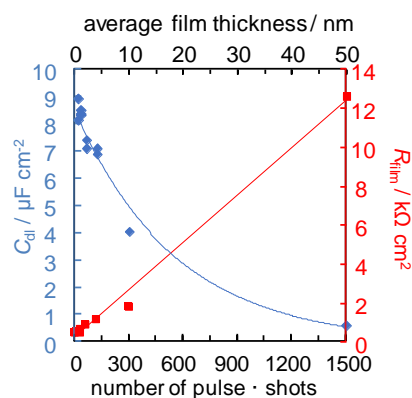


Fig. 1 Dependence of C_{dl} and R_{film} on film thickness of ZrO_x .

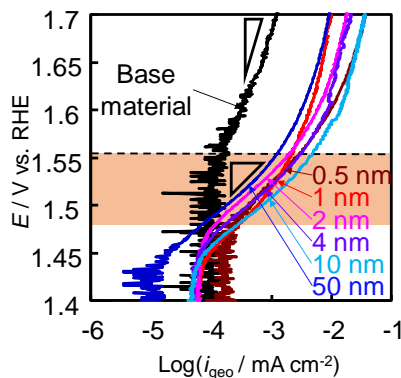


Fig. 2 Tafel plot on ZrO_x / Nb doped TiO_2 .

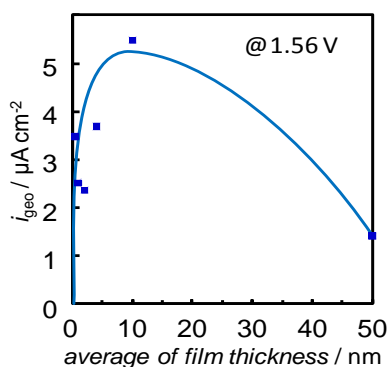


Fig. 3 Dependence of OER activities on film thickness of ZrO_x .

EFFECT OF ADDING Nb TO TITANIUM OXIDES AS NON-PLATINUM OXIDE-BASED CATHODES FOR PEFC

T. Tokai¹, A. Ishihara^{2*}, T. Nagai¹, Y. Kuroda¹, K. Matsuzawa¹, S. Mitsushima^{1,2}, and K. Ota¹

¹ Green Hydrogen Research Center, Yokohama National University (YNU), 79-5 Tokiwadai, Hodogaya-ku, Yokohama, 240-8501 Japan, cel2@ml.ynu.ac.jp

² Institute of Advanced Sciences, YNU, 79-5 Tokiwadai, Hodogaya-ku, Yokohama, 240-8501 Japan, cel2@ml.ynu.ac.jp

Keywords: Oxygen reduction reaction, PEFC, Non-platinum cathode, Titanium oxides, Crystal structure

INTRODUCTION

Polymer electrolyte fuel cell (PEFC) has already applied to a residential stationary power source and a power source for a fuel cell vehicles. However, platinum used as an electrode catalyst for PEFC is less resources and expensive, and its activity and stability as a cathode catalyst are insufficient. Therefore, in order to promote the spread of PEFC, it is necessary to develop a non-platinum catalyst alternative to a platinum, which is inexpensive, abundant in resources, high activity and durability. We have focused on group 4 and 5 transition metal oxides and have developed non-noble metal oxygen reduction catalysts [1]. Furthermore, in order to realize a non-carbon catalyst, we attempted to make a catalyst composed only of oxides. We successfully demonstrated that non-platinum and non-carbon catalyst was high durable at high potential [2]. However, these oxides had poor oxygen reduction reaction (ORR) activity and the factors affecting the ORR activity have not been clarified yet. Therefore, in this study, we have investigated the effect of adding Nb to titanium oxides to increase the ORR activity and to elucidate the factors affecting the ORR activity.

EXPERIMENTAL

Nb-doped titanium oxide powder (Nb-doped amount: 10 atm%) was made by high concentration sol-gel method [3] to prepare a precursor. The precursor powder was heat-treated in an electric furnace at 600-900 °C (Reduction temperature) for 10 min under reductive atmosphere, 4% H₂/Ar. Ketjen Black (KB) as a conductive substance with a weight ratio of 9 wt% was added to an obtained catalyst and the mixture was dispersed in a mixed solvent of 5 wt% Nafion® 6 μL and 1-hexanol 124 μL to make ink. The ink was dropped onto Glassy Carbon (GC) rod to load the catalyst powder of 0.10 mg and the rod after drying the solvent was used as a working electrode. We performed the electrochemical measurements used a three-electrode type cell in 0.1 mol dm⁻³ sulfuric acid at 30 ± 0.5 °C. The reference electrode was a reversible hydrogen electrode (RHE), and the counter electrode was a GC plate. Cyclic voltammetry was performed in nitrogen atmosphere with a scan rate of 150 mV s⁻¹ to stabilize the electrode surface. The potential was scanned between 0.2 V – 1.2 V vs. RHE in oxygen or nitrogen atmosphere with a scan rate of 5 mV s⁻¹ to obtain the ORR current.

RESULTS AND DISCUSSION

Fig. 1 shows the relationship between the ORR current at 0.7 V vs. RHE and the reduction temperature. In case of no addition of KB, all of the ORR current was almost zero. In case of the addition of KB, non-doped TiO₂ showed low activity from 600 to 900 °C. However, the ORR activity of Nb-doped TiO₂ was enhanced from 600 to 750 °C and had maximum activity at 700 °C even though its electrical conductivity was very low (ca. 10⁻⁶ S cm⁻¹). It means that the potential of Nb-doped TiO₂ emerged by a suitable reduction and the conductivity of the catalyst did not directly relate to the ORR activity.

Fig. 2 shows the relationship between the ratio of Anatase phase calculated from XRD patterns and the reduction temperature. A phase transition from Anatase to Rutile of the non-doped TiO₂ started from 600 to 650 °C. On the other hand, the Nb-doped TiO₂ started phase transition from 700 to 750 °C. It was well known that hetero-element doping suppressed the phase transition from Anatase to Rutile. Therefore, the suppression effect of Nb-doping TiO₂ was larger than that of non-doping TiO₂. According to the dependence of the ORR activity, Nb-doping is essential to have some ORR activity and the maximum ORR activity was observed just before the phase transition. It means that Nb-doped TiO₂ with Anatase phase showed high ORR activity by a suitable reductive heat-treatment.

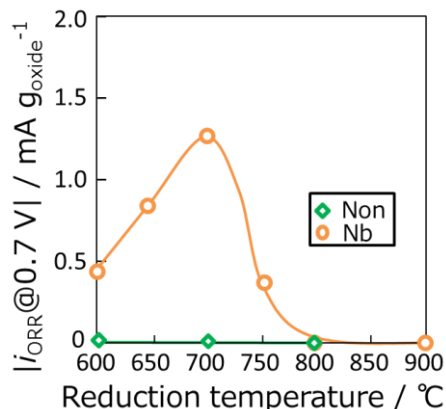


Fig. 1 Relationship between ORR current at 0.7 V vs. RHE and reduction temperature.

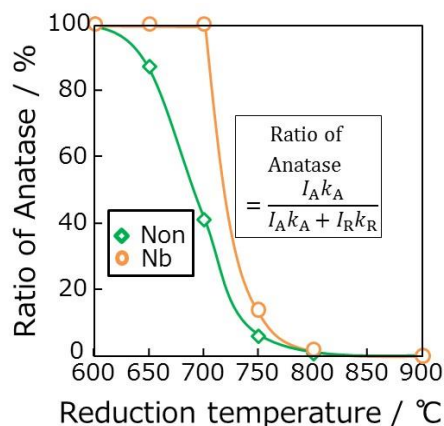


Fig. 2 Relationship between ratio of Anatase phase calculated from XRD patterns and reduction temperature.

REFERENCES

- [1] A. Ishihara, et al., J. Phys. Chem. C, 117, 18837 (2013).
- [2] M. Hamazaki, et al., Electrochemistry, 83, 817 (2015).
- [3] H. Matsuda, et al., J. Ceram. Soc. Japan, 107, 290 (1999).

ACKNOWLEDGEMENTS

The authors thank New Energy and Industrial Technology Organization (NEDO) for financial support. This work was also supported by the Izumi Science and Technology Foundation, Tonen General Sekiyu Research / Development Encouragement & Scholarship Foundation, and JSPS KAKENHI Grant Number JP18K05291. This work was conducted under the auspices of the Ministry of Education, Culture, Sports, Science and Technology (MEXT) Program for Promoting the Reform of National Universities.

NEW METHOD FOR EVALUATION OF POWDER OER CATALYSTS FOR AWE

Yudai Tsukada¹, Yoshiyuki Kuroda² and Shigenori Mitsushima³

¹ Green Hydrogen Research Center, Yokohama National University, tukada-yudai-rw@ynu.jp,

² Green Hydrogen Research Center, Yokohama National University, kuroda-yoshiyuki-ph@ynu.ac.jp,

³ Institute of Advanced Sciences, Yokohama National University, Green Hydrogen Research Center, Yokohama National University, mitsushima-shigenori-hp@ynu.ac.jp,

Keywords: LaNiO₃; alkaline water electrolysis; oxygen evolution reaction

INTRODUCTION

Highly active and durable electrocatalysts are demanded for hydrogen production by alkaline water electrolysis (AWE). We have reported high durability of LaNiO₃/Ni for oxygen evolution reaction (OER) under potential cycling¹, whereas it was difficult to evaluate their activity under practical current density (i.e. 600 mAcm⁻²). Many papers on powder anode catalysts for AWE have also been published to date, though most of them did not measure OER activity under such current density. For example, catalyst detachment occurs under relatively high current density, typically above 100 mAcm⁻² for drop cast catalysts on a glassy carbon (GC). Thermal decomposition method is useful to firmly attach catalysts on a metal electrode; however, oxide film with high resistance is formed between catalyst and electrode. In this study, we propose a new method for evaluation of OER activity of powder catalyst (LaNiO₃), attaching it on a metal electrode by cold isostatic press (CIP).

EXPERIMENTAL

LaNiO₃ powder (TOSHIMA, 99.9%) was pressed on an etched Ni or Ti substrate (The Nilaco corp., 99. +%) by CIP and used as a working electrode. That is, a LaNiO₃ powder ground on a mortar was dispersed in ethanol and ultrasonicated. The dispersion was painted on a substrate and subjected for pressurization by CIP at 300 MPa, followed by calcination at 650 °C for 60 min. The loading amounts were 11 and 126 mg cm⁻² on Ni, or 13 mg cm⁻² on Ti (denoted as CIP_11_Ni, CIP_126_Ni and CIP_13_Ti). Counter and reference electrodes were a Ni coil and a reversible hydrogen electrode (RHE), respectively. All measurements were performed in a three-electrode electrochemical cell at 30±1°C in 7.0 M (= mol dm⁻³) KOH. Cyclic voltammetry for 100 cycles between 0 and 1.0 V vs. RHE with the scan rate of 100 mVs⁻¹ was applied as electrochemical pretreatment. The catalytic activity of the OER was evaluated by cyclic voltammetry between 0.5 and 2.3 V vs. RHE with the

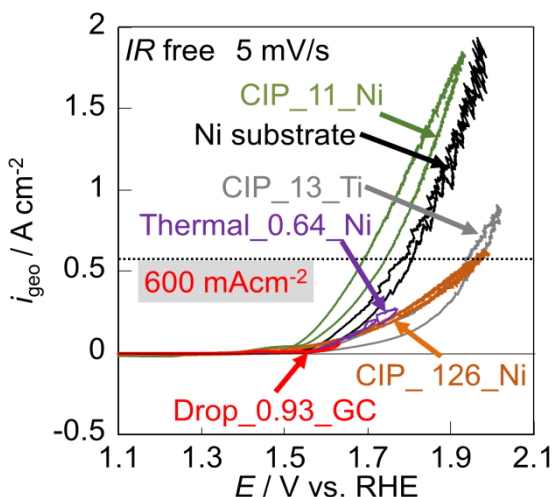


Fig.1 Polarization Curves of OER on each electrodes

scan rate of 5 mVs^{-1} . The resistance of surface oxide film (R_f) was evaluated by the AC impedance spectroscopy with higher frequency arc at 1.6 V vs. RHE.

RESULTS AND DISCUSSION

Figure 1 shows the iR free polarization curves of the electrodes prepared by different catalyst immobilization methods, where the R (electrolyte resistance) is the higher frequency intercept on the real axis. The polarization curves without electrochemical pretreatment are shown for the electrodes by drop cast and thermal decomposition methods, whereas those with the pretreatment were shown for electrodes prepared by CIP. The maximum current density was 50 mA cm^{-2} for the electrode prepared by drop cast because catalyst was detached from substrate by oxygen bubble under higher current density. In spite of this limited current density, the OER current density decreased every cycle, meaning its catalytic activity was not accurately evaluated. On the other hand, current densities of the electrode by CIP was stable during potential cycling above 600 mA cm^{-2} . Figure 2 shows loading amount of LaNiO_3 before and after electrochemical measurement. The loading amount of the electrode prepared by drop cast decreased in 66%, though those of the electrodes prepared by CIP were decreased in 2–35%. It means that catalysts were more stably immobilized by the CIP method.

Figure 3 shows oxide film resistance on each electrode. The oxide film resistances of CIP electrodes were lower than half value of the resistance of the electrode prepared by thermal decomposition. The formation of NiO on a Ni substrate due to longer calcination time is the reason for the high oxide film resistance of the electrode prepared by the thermal decomposition.

Therefore, CIP is suitable for the evaluation of OER activity under practical current density, such as 600 mA cm^{-2} , because of the suppression of catalyst detachment and low oxide film resistance.

REFERENCES

- [1] Y. Tsukada et al., 232nd ECS meeting, USA (2017).

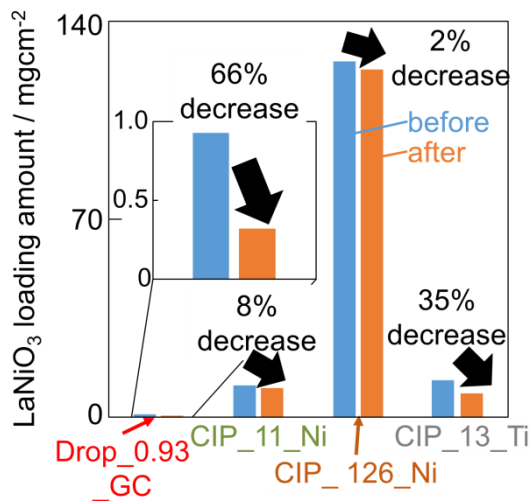


Fig.2 LaNiO_3 loading amount before and after electrochemical measurement

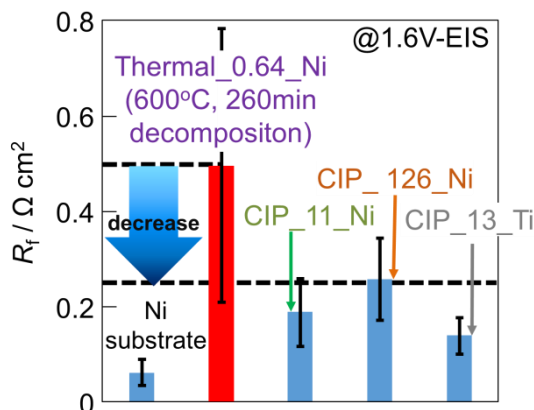


Fig.3 Oxide film resistance on each electrodes

IN SITU ELECTROCHEMICAL CHARACTERIZATION OF LOW-TEMPERATURE PEM DIRECT ETHANOL FUEL CELLS USING DC AND AC METHODS

Paweł Wnuk¹, Adam Lewera², Rafał Jurczakowski³

¹ University of Warsaw, Department of Chemistry, Biological and Chemical Research Centre, Warsaw, Poland. pwnuk@chem.uw.edu.pl

² University of Warsaw, Department of Chemistry, Biological and Chemical Research Centre, Warsaw, Poland. alewera@chem.uw.edu.pl

³ University of Warsaw, Department of Chemistry, Biological and Chemical Research Centre, Warsaw, Poland. rafjur@chem.uw.edu.pl

Keywords: PEM Fuel Cells, Ethanol Electrooxidation, Impedance Spectroscopy, Platinum

Low-temperature Direct Ethanol Fuel Cells with Polymer Electrolyte Membrane (PEM DEFC) are considered a promising energy source for the future. Ethanol is a potentially good fuel for fuel cells with many advantages, such as ease of production and transportation, high energy density and thermodynamic efficiency. However, low activity of currently known ethanol electrooxidation catalysts and their poor selectivity towards full oxidation to carbon dioxide are impeding the progress in development of PEM DEFC. The highest reported cell power densities (up to ca. 100 mW·cm²) are too low for practical applications and more importantly, no significant improvements of power density have been made in the recent years. [1] Due to the complex mechanism of ethanol electrooxidation, most up-to-date electrochemical studies regarding catalysts for DEFC are conducted in *ex situ* conditions, which are easier to interpret than *in situ* measurements. On the other hand, only *in situ* studies reflect influence of different cell operating parameters and all occurring phenomena, including by-processes, such as cross-over of fuels through the Nafion membrane.

Impedance spectroscopy is a technique that has proven useful for *in situ* investigation of low-temperature PEM fuel cells fed with hydrogen, methanol or formic acid. [2,3,4] However, reports on *in situ* impedance studies of PEM DEFC in the literature are scarce and limited to a narrow range of frequency and cell parameters. [5,6] This contribution presents a systematic investigation of PEM DEFC with electrodes containing platinum-based catalysts using *in situ* DC (I-E characteristics) and AC (impedance spectroscopy) electrochemical methods. Constant flow of reactants in the investigated cells assured a stationary state, which isn't easily acquired in *ex situ* conditions and allowed for obtaining reproducible results of experiments. [7] Because the cell was operated in steady state conditions, indicated by no changes of cell voltage over time, the impedance spectra could be registered in wide range of perturbation frequency – down to 1 mHz. Measurements at such low frequencies revealed phenomena related to adsorption of reaction intermediates, characterized by large relaxation time constants, that are not observable in typical frequency range applied in fuel cell studies (down to ca. 10 mHz). Influence of different catalyst composition and cell operating conditions on the cell properties has been studied. A qualitative and quantitative interpretation of the obtained data is presented, based on the parameters obtained from equivalent electrical circuits proposed for modelling the recorded spectra.

REFERENCES

- [1] S.P.S. Badwal, S. Giddey, A. Kulkarni, J. Goel, S. Basu, *Appl Energ* Vol. 145 (2015), p. 80 - 103
- [2] P. Piela, R. Fields, P. Zelenay, *J Electrochem Soc* Vol. 153 (2006), p. A1902 - A1913
- [3] S.M.R. Niya, M. Hoorfar, *J Power Sources* Vol. 240 (2013), p. 281 - 293
- [4] S. Uhm, S.T. Chung, J. Lee, *J Power Sources* Vol. 178 (2008), p. 34 - 43
- [5] P. Ekdharmasuit, A. Therdthianwong, S. Therdthianwong, *Int J Hydrogen Energ* Vol. 39 (2014), p. 1775 - 1782
- [6] S.C. Zignani, V. Baglio, J.J. Linares, G. Monforte, E.R. Gonzalez, A.S. Arico, *Int J Hydrogen Energ* Vol. 38 (2013), p. 11576 – 11582
- [7] C. Desilets, A. Lasia, *Electrochim Acta* Vol. 78 (2012), p. 286 - 293

THE EFFECT OF PREPARATION CONDITIONS OF $\text{Li}_x\text{Ni}_{2-x}\text{O}_2/\text{Ni}$ ON ELECTROCHEMICAL PERFORMANCE FOR ALKALINE WATER ELECTROLYSIS

Xu Yao¹, Yoshiyuki Kuroda¹, Ikuo Nagashima², Yoshinori Nishiki³, Shigenori Mitsushima¹

¹ Green Hydrogen Research Center, Yokohama National University, 79-5 Tokiwadai, Hodogaya-ku, Yokohama 240-8501, Japan

² Kawasaki Heavy Industries, Ltd., 1-1 Kawasaki-cho, Akashi, 673-8666, Japan

³ De Nora Permelec, Ltd, 2023-15, Endo, Fujisawa City, Kanagawa 252-0816 Japan

E-mail: cel@ml.ynu.ac.jp

Keywords: Alkaline water electrolysis, Oxygen evolution reaction, Li doped nickel oxide

INTRODUCTION

Alkaline water electrolysis (AWE) is a suitable commercial production method for “Green hydrogen” that is made from water and renewable energy with a simple and less expensive configuration. A conventional AWE anode is Ni based material which is stable under steady electrolysis [1]. However Ni is prone to be deteriorated under cycling potential which simulated fluctuating electricity from renewable energies, the durability of Ni based anode needs improvement. In previous study, we developed $\text{Li}_x\text{Ni}_{2-x}\text{O}_2/\text{Ni}$, prepared by thermal decomposition with acetate, had not only a high electric conductivity and high activity but also high durability, because of the modification of nickel by a dense $\text{Li}_x\text{Ni}_{2-x}\text{O}_2$ layer [2]. To prepare $\text{Li}_x\text{Ni}_{2-x}\text{O}_2/\text{Ni}$ electrode with both high activity and durability, the effect of preparative conditions should be investigated.

EXPERIMENTAL

A Ni plate (The Nilaco Co., 99+%) was used as a base substrate which was etched in boiling 17.5 % hydrochloric acid for 6 min. A butanol solution of LiNO_3 and $\text{Ni}(\text{CH}_3\text{COO})_2 \cdot 4\text{H}_2\text{O}$ was used as a precursor. The precursor was painted, dried at 80 °C for 15 min, and thermally decomposed at 550 °C for 15min. After repeating the procedure for several times, the electrode was calcined at 550 °C for 1h. $\text{Li}_x\text{Ni}_{2-x}\text{O}_2$ was coated by two methods, painting by hand and by automated painting device (Santekku Corp.). In the hand-painting experiments, the Li/Ni ratio was varied as $x = 0.10$ (Li@0.10), 0.12 (Li@0.12), and 0.14 (Li@0.14) to investigate the effect of the Li/Ni ratio. To investigate the difference of two preparation methods, the coating of $\text{Li}_x\text{Ni}_{2-x}\text{O}_2$ by automated painting device, the x value was fixed to 0.14 (Li@0.14(Auto)). By automated painting device, the morphology of the film was changed by adding 1% (Li@0.14(Auto-1%Alc.)), 5% (Li@0.14(Auto-5%Alc.)) 10%(Li@0.14(Auto-10%Alc.)) 1-propanol to precursory solution.

A Ni coil and a reversible hydrogen electrode (RHE) were used as counter and reference electrodes, respectively. All electrochemical measurements were performed, using three-electrode cell at 30 °C with 7.0 M ($=\text{mol dm}^{-3}$) of KOH as an electrolyte. The durability was examined by 20,000 cycles of potential sweeps between 0.5 and 1.8 V vs. RHE with the scan rate of 1 V s^{-1} . The OER activity was measured by slow scan voltammetry (SSV) between 0.5 and 1.8 V vs. RHE with the scan rate of 5 mV s^{-1} .

RESULTS AND DISCUSSION

Fig. 1 shows dependence of the OER current density during potential cycling for the $\text{Li}_x\text{Ni}_{2-x}\text{O}_2/\text{Ni}$ electrodes with various Li-doped contents. In the initial period of the durability test, the oxide films with higher Li-doped amount exhibited higher current density probably because of increased conductivity. The oxide films with lower Li-doped amount showed higher durability than a bare Ni. Thus, Li@0.10 had the highest activity and durability after 5000 cycles in this study. From X-ray photoelectron spectroscopy, the Li@0.10 showed remaining of more NiO after durability test than other electrodes. Li@0.14(Auto) exhibited higher activity and durability than Li@0.14 possibly because of the formation of a denser and thinner oxide film.

Table 1 shows the variation of film thickness for the electrodes made from various precursor solutions.

When 1-propanol was added in the precursor solution, the surface morphology became flat and thickness increased because of higher wettability. Li@0.14(10%Alc.) had the highest resistance because of the largest thickness. After durability test, the change in the film thickness for Li@0.14(5%Alc.) and Li@0.14(10%Alc.) were larger than the others probably because more oxide film was peeled off or dissolved during the durability test. Figure 2 shows durability of the OER current density during potential cycling for the electrodes made from various precursor solutions. Li@0.14 (Auto-5%Alc.) exhibited higher activity at the initial stage of the durability test because of the high conductivity. Li@0.14(H_2O) had the highest activity and durability after 3000 cycles. Not only because the oxide film was more stable, but also the small charge transfer resistance was observed. Thus, it was found that the coating method and conditions are important for the improvement of the durability of OER electrodes.

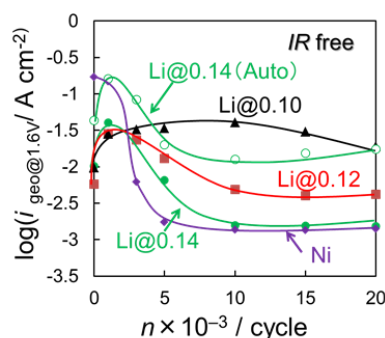


Fig. 1 OER current density during potential cycling of the electrodes with different Li-doped content at 1.6V vs. RHE

Table 1. Film thickness of the electrodes ($x = 0.14$).

Sample	Before durability test / μm	After durability test / μm
Auto- H_2O	4.2	2.7
Auto-1%Alc.	6.1	5.1
Auto-5%Alc.	4.4	1.0
Auto-10%Alc.	7.3	1.5

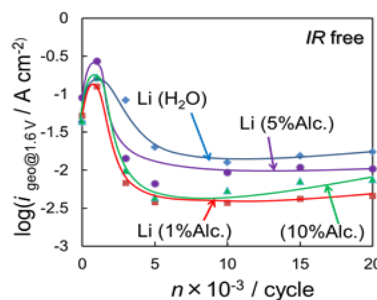


Fig. 2 OER current density during potential cycling of the electrodes with different precursor solution at 1.6V vs. RHE

- [1] P. W. T. Lu and S. Srinivasan. *J. Electrochem. Soc.*, **125** (1978) 1416–1422/
 [2] S. Fujita, I. Nagashima, Y. Nishiki, C. Canaff, T. W. Napporn, S. Mitsushima, *Electrocatalysis*, **9** (2018) 162-171.

DEVELOPMENT OF IRON BASED OXYGEN CARRIERS FOR CHEMICAL LOOPING HYDROGEN

Robert Zacharias¹, Sebastian Bock¹, Viktor Hacker¹

¹ Institute of Chemical Engineering and Environmental Technology, Graz University of Technology, Austria

Keywords: Chemical looping hydrogen, oxygen carrier synthesis, thermogravimetric analysis

INTRODUCTION

An economy based on hydrogen, utilizing fuel cells offers the chance for a carbon dioxide free electric power supply. The ecological footprint of hydrogen as a secondary energy carrier largely depends on the production method. At the time, the main production method is steam reforming of hydrocarbons in large-scale centralized plants, which emits a high amount of greenhouse gases. Decentralized hydrogen production via fixed bed chemical looping in contrast has no need for long distance truck transports and utilizes renewable feedstock. The process consists of the cyclic reduction and oxidation of an iron oxide based oxygen carrier (OC). In the first step, synthesis gas out of biofuels or methane is used to reduce the oxygen carrier at 800 °C, followed by the production of hydrogen through the oxidation of the OC with steam. High process efficiencies of up to 80% have been published [1], [2].



A critical issue is the development of suitable oxygen carrier materials, as the use of pure iron oxide leads to a fast decrease of the oxygen exchange capacity (OEC) and therefore a decreasing hydrogen production over time [4]. For the industrial application of the process the long-term stability of the OEC is crucial to be economical [5]. For that reason, chemical synthesis methods were employed to improve the material structure towards resistance to agglomeration and accordingly improved long-term stability.

METHODS

Oxygen carriers materials consisting of 70-90% Fe₂O₃ stabilized with the corresponding amount of Al₂O₃ were prepared by mechanical mixing (MM) and wet chemical synthesis (CS) [3]. The reaction products were crushed, calcined and milled to a final particle size of <90 µm. Approximately 40 mg of the sample were placed on the plate sample holder of a Netzsch STA 449c simultaneous thermal analyzer equipped with a steam generation furnace. Stability tests consisted of 30 minutes reduction amidst a total gas flow of 100 ml min⁻¹ of an equimolar mixture of H₂ and N₂, followed by 30 min oxidation with 3.6 g min⁻¹ steam supply and 50 ml min⁻¹ N₂ carrier gas flow.

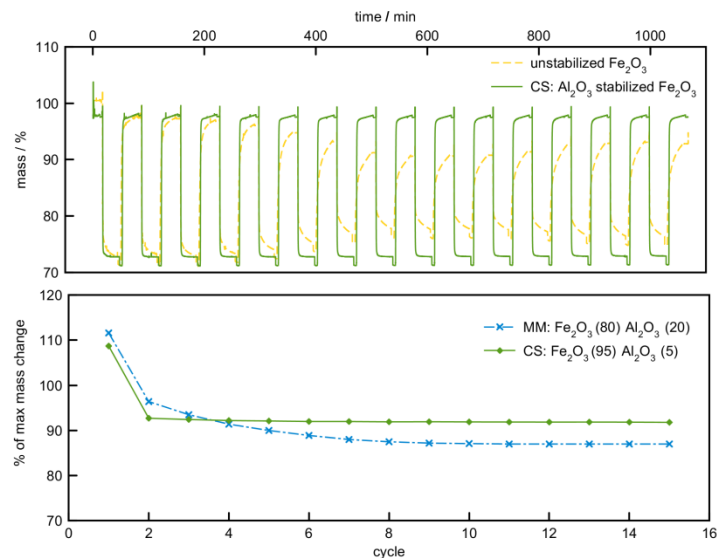


Fig. 4: Evaluation of mass stability over time a) unstabilized Fe_2O_3 vs. CS; b) CS vs. MM

RESULTS

Results of thermogravimetric stability tests are shown in Fig 1. Part (a) outlines the high stabilizing effect of alumina compared to an unsupported Fe_2O_3 sample. Pure Fe_2O_3 powder suffers from a fast decrease of the OEC and therefore a poor performance starting with the third cycle. The grey curve that represents the OC synthesized with CS (Al_2O_3 supported) showed no degradation over the whole measurement. Reason for the enormous decrease of the unstabilized sample is a shrinking surface area because of sintering, as BET surface area measurements showed. Oxygen carrier samples made with CS exceeded MM samples in the stability of the OEC over time (Fig 1, b). The share of support material and its distribution inside the OC are two crucial points to gain stability and reactivity and are primarily influenced by the synthesis method. Long-term stability of the OC material is an essential requirement for the successful commercialization of the process. Therefore, ongoing investigations deal with long-term thermogravimetric stability tests of promising samples. Therefore, samples with highest OEC stability were selected and further compared with tests for up to 330 reduction and oxidation cycles.

ACKNOWLEDGEMENTS

Financial support by the Klima- and Energiefonds through the Energy Research Program 2015 is gratefully acknowledged.

REFERENCES

- [1] V. Hacker, J. Power sources, Vol. 118 (2003), pp. 311–314
- [2] S. D. Fraser, M. Monsberger, and V. Hacker, J. Power Sources, Vol. 161 (2006), pp. 420–431
- [3] C. D. Bohn, J. P. Cleeton, S. A. Scott, J. S. Dennis, C. R. Müller, S. Y. Chuang, Energy & Fuels, Vol. 24 (2010), pp. 4025–4033.
- [4] G. Voitic, V. Hacker, RSC Adv., Vol.6 (2016), pp. 98267–98296
- [5] M. Luo, Y. Yi, S. Wang, Z. Wang, M. Du, J. Pan, and Q. Wang, Renew. Sustain. Energy Rev., vol.81 (2018), pp. 3186–3214.

Keynote Speakers

Prof. Dario DEKEL, Technion, Israel Institute of Technology, Haifa, Israel

Dr. Michael GÖTZ, ElringKlinger, Dettingen/Erms, Germany

Dr. Reinhard TATSCHL, AVL List, Graz, Austria

Prof. Ken-Ichiro OTA, Yokohama National University, Japan

4th International Workshop on Hydrogen and Fuel Cells

within the 11th International Summer School on Advanced
Studies of Polymer Electrolyte Fuel Cells

August 23rd 2018

Institute of Chemical Engineering
and Environmental Technology, NAWI Graz
Graz University of Technology,
Inffeldgasse 25c, 8010 Graz, Austria

All rights reserved

Financial support was provided by the Austrian Ministry for Transport, Innovation and Technology, the Climate and Energy Fund of the Austrian Federal Government and the Austrian Research Promotion Agency (FFG) through the IEA Research Cooperation.

